Università degli Studi di Padova
DEPARTMENT OF INFORMATION ENGINEERING

Master Degree in Telecommunication Engineering

Master Thesis

Discrimination of strain and temperature in Brillouin Optical Time Domain Analyzers via Artificial Neural Networks

Author: Arianna Piccolo

Supervisor: Galtarossa, Andrea

Tutor at UNICAN: Mirapeix Serrano, Jesús María

ACADEMIC YEAR 2015 - 2016

10 October 2016

Abstract

Civil structures and constructions, buildings, bridges, dams, high-voltage power lines, etc. have an essential role in human life. It is then desirable to control their health in order to avoid malfunctioning or breaks, before accidents happen putting at risk those infrastructures and, ultimately, people's life. It is however often complicated to monitor big constructions, due to their size but also because damages usually start from the inside of the structure, where they can not be seen.

To this purpose, the use of *Distributed Optical Fiber Sensors* (Distributed OFSs) is of big help, since using a single fiber it is possible to investigate many kilometers of a bridge, a building or a cable. Distributed OFSs are developed exploiting scattering processes like Rayleigh, Raman or Brillouin scattering.

In this work, *stimulated Brillouin scattering* (SBS) is used, working with a *Brillouin Optical Time Domain Analysis* (BOTDA) configuration, in order to retrieve the *Brillouin Gain Spectrum* (BGS) along the *Fiber Under Test* (FUT). In fact, it is known that the BGS of a fiber depends, spatially, not only by its material characteristics but also on the state in which the fiber is found, like if it is under temperature or strain effects. In this way, analyzing differences of various BGSs obtained by different fiber situations, it could be possible to understand which kind of modification the fiber is suffering, knowing the dependence of fiber characteristics with temperature and strain. This is a crucial aspect for health monitoring: understand if the fiber is being heated or stressed is of high importance if a fast and mindful restore operation is required.

The goal of this thesis, in fact, is the achievement of a method able to obtain a discrimination between temperature and strain effects that can occur simul-

taneously on the fiber. The procedure to reach the target is the following: a fiber was set under temperature and/or strain changes, performing then distributed BOTDA measurements and getting many BGSs, which constitute useful informations to distinguish which is the cause, temperature, strain or both, that gives such particular Brillouin profile. Since standard BOTDA measurements are not able to reach this discrimination goal, a different way to work with BGSs had to be developed.
In order to analyze in an automatic way these BGSs, a computing tool was necessary. The choice fell on *Artificial Neural Networks* (ANNs), a computing tool deriving from deep learning paradigms. Exploiting their capacity to learn from examples and generalize their structure to be used for different but consistent measurements, it was possible to let them decide which effect was occurring onto the fiber. Trying with different ANN configurations and ways to give them inputs, different success percentages are obtained, reaching a maximum of more than 70% in some cases for both strain and temperature selection and a unique 86.7% of success for strain selection using a particular way to test and analyze the outcomes.
This work, that can be understood as a feasibility study, may give rise to an interesting and promising research line, giving new improving possibilities to this important subject.

Keywords: Fiber optics, Fiber optic sensors, Distributed sensing, Brillouin scattering, Stimulated Brillouin Scattering, BOTDA, Temperature and Strain Discrimination, Artificial Neural Networks

Acknowledgments

This thesis is the result of a long work and, above all, an adventure.
All started when I seized the opportunity to do my Master Thesis in a foreign Country, with the Erasmus+ program, even if I never truly believed I was the right person to face such an experience.
I would like to thank all the people who motivated me, cheered me up and helped me to win my fears, exploit my potential and grow up as a human being, personally and professionally.
First of all, I would like to thank the person who convinced me to take this opportunity, that later became my supervisor, Professor Andrea Galtarossa, who always believed in me and supported me to work at my best, even in tougher times.
Secondly, I would like to thank all the guys who welcomed me as one of the Photonic Engineering Group of University of Cantabria in Santander, Spain, starting from Professor José Miguel López-Higuera, Head of the group, who tried his best to make me feel home. I would like to thank Chus, who did a more than awesome job as tutor, supporting me with friendship and Rubén, who followed me in the laboratory. I also would like to thank Arturo, Luis, Eusebio, Iñaki, Marina, David, Hany, Maria, Javi and everyone in the group who accompanied me in this journey. *Muchas gracias a todos, ¡os quiero!*
I would like of course to thank all my friends who always stayed by my side, no matter what, how or why. You know who you are.
Finally I would like to thank my relatives and, mostly, my family, my mom Marinella, my dad Alberto, my sister Veronica and Achille. You always supported me through all my life and I could not be more thankful for helping me becoming who I am now.

This work has been co-supported by project TEC2013-47264-C2-1-R.

Contents

List of Figures

1

Introduction/Introduzione

English

1.1 Context

Optical fibers are one of the most important and promising technologies developed in the XX century. Firstly found to be useful for communication systems, still used now as communication medium or as a base for other optical devices (amplifiers, filters, etc.), they assumed a whole new role as sensors, thanks to researches of the last 30 years, in many different fields (medicine, civil engineering, industry, etc.).
Sensors are one of the most recent optical fiber-based technologies, which are mainly divided into two categories: point sensors, like a single fiber Bragg grating (FBG), or distributed sensors (or multipoint), that exploit the whole fiber thanks to scattering processes that can be linear, like Rayleigh, or non-linear, like Raman and Brillouin.
Why are these particular scattering processes so interesting for sensor systems? The wavelength, the shape and the intensity of the scattered light spectrum depend not only on the characteristics of the intrinsic material but also on the changes of the environment that surrounds the fiber. Strain and temperature can be then distributedly measured by analyzing the spectrum of the scattered light at one end of the fiber.
This thesis is focused on Brillouin distributed sensing systems and, in particular, on Brillouin optical time domain analyzers. In fact, there are many

setups based on the Brillouin scattering process, where interactions between acoustic and optical waves take place within the fiber. This acoustic wave acts as a moving grating, scattering incident light under energy and momentum conservation laws [1].
The Brillouin scattering can be spontaneous, where acoustic phonons are thermally excited, or stimulated, where two light waves, having a frequency difference near the Brillouin one, counter-propagate in the fiber, thus stimulating the creation of the acoustic wave. The first one is at the base of the Brillouin optical time domain reflectometry (BOTDR) while the latter is responsible for the Brillouin optical time domain analysis (BOTDA). There are also other Brillouin-based systems, like BOFDA (in the frequency domain) and BOCDA (in the correlation domain), however the main focus of this thesis is on BOTDA, especially on the setup proposed by M. A. Soto and L. Thévenaz in [2].

1.2 Goals

As already mentioned, Brillouin scattering is sensitive to both strain and temperature, so one of the most important and critical things to understand what is occurring to the fiber (and so to the surroundings), is to be able to discriminate the effect of these two events. In fact, both influence the Brillouin maximum gain frequency (called also Brillouin frequency shift, BFS) and the scattered light amplitude, however it has been highlighted how these two phenomenons give rise to slightly different Brillouin gain spectrum (BGS) changes [3].
Exploiting these differences it might be then possible to discriminate strain and temperature and researchers have found different ways to do it: using two scattering processes together, special fibers or particular ways to embed the fiber on the sensing support. In this thesis a different proposal will be explored, using artificial neural networks (ANNs).

ANNs are computing models inspired by the structure and function of the biological neural network, the human brain: networks of highly parallel-interconnected systems, consisting of basic computational units or *neurons* arranged in layers. When a neuron in the network receives weighted input signals, it 'fires' or produces an output if the sum of the inputs exceeds the internal threshold level for that neuron [4].
An ANN operates mainly in two phases: the first one where the network is trained and the second when it is tested. In the training phase, input-output couples of samples are fed to the network and, depending on the selected algorithm, the weights of the network are adjusted until the resulting output is sufficiently close to the desired one. Once this goal is reached, the test phase can begin, where only inputs are given to the network. If the training has been good enough, the correct output will be chosen.
In this way, ANNs can be used for the purpose of this thesis: after a proper training, an ANN should be able to properly distinguish the effect of only strain, only temperature or even to quantitatively establish the simultaneous participation of both (at a given location of the sensing fiber).
In order to better understand the context, the work done and to have a panoramic of this field, this thesis has been divided into the following sections: Chapter 2 is dedicated to an overall explanation and discussion over the state of the art of distributed fiber optic sensors and more specifically of BOTDAs; Chapter 3 is focused on ANNs, going more in details on their history and how they work; on Chapter 4 it is then showed the experimental setup, describing its different elements and how and why it works; finally on Chapter 5 the attention is given to how the laboratory tests are performed and which results are obtained, that will be the main focus of Chapter 6, dedicated to the conclusions and future research.

Italiano

1.3 Contesto

Le fibre ottiche sono una delle più importanti e promettenti tecnologie sviluppate nel XX secolo. Inizialmente utili per sistemi di comunicazione, usate ancora oggi come mezzo di comunicazione o come base da cui partire per altri dispositivi ottici (amplificatori, filtri, ecc.), hanno assunto un nuovo ruolo come sensori, grazie alle ricerche degli ultimi 30 anni, in vari ambiti diversi (medicina, ingegneria civile, industria, ecc.)
Quella dei sensori è una delle più recenti tecnologie sviluppate basate su fibra ottica e sono principalmente divisibili in due categorie: sensori puntuali, come un singolo reticolo di Bragg in fibra (FBG), o sensori distribuiti (o multipoint), che sfruttano l'intera fibra grazie a processi di diffusione (scattering) che possono essere lineari, come quello di Rayleigh, o nonlineari, come quelli di Raman e Brillouin.
Perché questi processi di scattering sono così importanti per i sistemi di sensori? La lunghezza d'onda, la forma e l'intensità dello spettro della luce diffusa dipendono non solo dalle caratteristiche del materiale intrinseco ma anche dalle variazioni dell'ambiente che circonda la fibra. Strain e temperatura possono essere quindi misurate in maniera distribuita analizzando lo spettro della luce diffusa ad un capo della fibra.
Questa tesi è incentrata su sistemi di sensori distribuiti che utilizzano lo scattering di Brillouin e, in particolare, sulla configurazione BOTDA (Brillouin optical time domain analyzers) nel dominio del tempo. Infatti, esistono molti sistemi basati sullo scattering di Brillouin, per cui interazioni tra onde acustiche e ottiche avvengono all'interno della fibra. L'onda acustica agisce da reticolo mobile, diffondendo la luce incidente in base alle leggi di conservazione di energia e momento [1].
Lo scattering di Brillouin può essere spontaneo, dove i fononi acustici sono eccitati termicamente, o stimolato, dove due onde luminose, aventi differenza

di frequenza vicina a quella di Brillouin, si propagano in direzioni opposte nella fibra, stimolando così la creazione dell'onda acustica. Il primo è alla base del Brillouin optical time domain reflectormetry (BOTDR) mentre il secondo è responsabile del Brillouin optical time domain analysis (BOTDA). Ci sono inoltre altri sistemi basati su Brillouin, come BOFDA (nel dominio della fequenza) e BOCDA (nel dominio della correlazione), in ogni caso il focus di questa tesi è sul BOTDA, specialmente sul setup proposto da M. A. Soto e L. Thévenaz in [2].

1.4 Obiettivi

Come già menzionato, lo scattering di Brillouin è sensibile a cambi di strain e temperatura, dunque una delle cose più importanti e cruciali per capire cosa stia succedendo alla fibra (e quindi all'ambiente circostante), è l'essere in grado di discriminare l'effetto di questi due eventi. Infatti, entrambi influenzano la frequenza di massimo guadagno di Brillouin (chiamata anche Brillouin frequency shift, BFS) e l'ampiezza dello spettro luminoso diffuso, però è stato evidenziato come questi due fenomeni danno luogo a spettri di guadagno di Brillouin (BGSs) leggermente diversi quando il loro valore cambia [3].
Sfruttando queste differenze potrebbe essere possibile allora discriminare gli effetti di strain e temperatura e i ricercatori hanno scoperto diversi metodi per farlo: usando due processi di scattering insieme, fibre speciali o particolari modi di incorporare la fibra sul supporto desiderato. In questa tesi una diversa proposta verrà esplorata, sfruttando le reti neurali artificiali (artificial neural networks, ANNs).
Gli ANNs sono modelli computazionali ispirati dalla struttura e funzione della rete neurale biologica, il cervello umano: sono reti di sistemi altamente connessi in parallelo, che consistono di unità computazionali base o *neuroni* organizzati a strati (*layers*). Quando un neurone della rete riceve un segnale

con un certo *peso* in ingresso, "spara" o produce un output se la somma degli input eccede il livello di soglia interna per quel neurone [4].
Un ANN opera principalmente in due fasi: la prima dove la rete viene allenata (fase di *training*) e la seconda dove viene testata (fase di *test*). Nella prima, coppie di input-output sono date in pasto alla rete e, in base all'algoritmo scelto, i pesi della rete vengono regolati fino a quando l'output risultante è sufficientemente vicino a quello desiderato. Una volta che lo scopo è raggiunto, la fase di test può cominciare, nella quale solo input sono dati alla rete. Se il training è stato abbastanza buono, l'output giusto verrà selezionato. In questo modo, le reti neurali possono essere usate per lo scopo di questa tesi: dopo un corretto allenamento, una rete dovrebbe essere in grado di distinguere adeguatamente l'effetto di solo strain, solo temperatura o addirittura stabilire la partecipazione simultanea di entrambi (per una data posizione nella fibra).
Per comprendere meglio il contesto, il lavoro svolto e avere una panoramica di questo campo di ricerca, questa tesi è stata divisa nelle seguenti sezioni: il Capitolo 2 è dedicato ad una spiegazione e discussione complessiva sullo stato dell'arte dei sensori distribuiti in fibra ottica e più specificamente dei BOTDAs; il Capitolo 3 è incentrato sugli ANNs, entrando maggiormente nei dettagli sul loro funzionamento; nel Capitolo 4 è mostrata l'attrezzatura sperimentale, descrivendone i diversi componenti e come e perché funziona; infine nel Capitolo 5 l'attenzione è rivolta a come i test in laboratorio sono stati effettuati e quali risultati sono stati ottenuti, i quali sono il principale focus del Capitolo 6, dedicato alle conclusioni e agli sviluppi futuri.

2

Brillouin distributed fiber optic sensors: state of the art

Brillouin distributed fiber optic sensors are just one of the many fiber based sensors that can be used, studied and analyzed nowadays.
The first experiments on low-loss optical fibers used as sensors literally saw the light in the early 1970s, while the interest has been raising until now thanks to the possibility of being utilized in difficult measurement situations where conventional sensors (on coaxial cable or electronic devices) can not be used or exhibit a poorer performance. In fact silica optical fibers have a lot of advantages as being lightweight, of very small size, passive, low power, resistant to electromagnetic interferences, high sensitivity, wide bandwidth, and environmental ruggedness. Their disadvantages, as being high cost and by now unfamiliar to the end user, are year by year less important thanks to the numerous groups working in the field from all over the world.
There are two main fiber optic sensor types: the point and the distributed ones. Point sensors are those in which measurements are taken in single locations in space, where the sensing element is typically positioned at or near the end of an optical fiber, that is used as a link between the sensing element and the light source/interrogator. There are also other point sensors however, like FBGs, where the sensing element is the optical fiber: for the FBG, the fiber must be properly exposed to UV light in order to change periodically the refractive index of the core and thus creating a grating inside the fiber. The particular UV exposure affects the properties of the grating, especially

the intensity and duration of the exposure as well as the photosensitivity of the fiber. Photosensitivity is a nonlinear effect that initially was thought to be a phenomenon associated only with germanium doped optical fibers. Subsequently, it has been observed in a wide variety of different fibers, many of which did not contain germanium as a dopant. Photosensitivity can also be enhanced by pre-soaking the fiber in hydrogen, however germanium doped fibers remain the most important material for the fabrication of these devices [5]. The change in refractive index is permanent under normal conditions, in the sense that it will last for decades (lifetimes of 25 years are predicted) if the optical waveguide after exposure is annealed appropriately, that is by heating for a few hours at a temperature of 50 °C above its maximum operating temperature.

The FBG reflects light having a wavelength equal to $\lambda_B = 2n_{eff}\Lambda$, where n_{eff} is the modal index and Λ is the grating period. The sensing can thus be performed by observing the scattered light wavelength from the FBG, since the grating period can be modified by strain occurrence or temperature changes in the fiber.

According to this, FBGs are suitable for many different applications, although there are some obvious limitations associated with point sensors, making them unsuitable to some scenarios such as long range monitoring of civil engineering infrastructures, pipelines or high-voltage power lines, just to mention some examples. Distributed fiber sensor systems then, where the whole fiber itself is employed as the sensing element, may overcome these limitations and, therefore, give rise to an improved performance.

In this thesis the main focus is on Brillouin distributed fiber optic sensors, especially on BOTDA implementations, however a brief overview on the most significant distributed sensing systems will be here considered, going increasingly towards the BOTDA system used in this thesis for the measurements.

2.1 Distributed fiber optic sensors

Distributed sensors systems are the perfect choice when it is necessary to monitor a whole big structure, like buildings, airplanes, dams, bridges, pipelines, etc., in order to be able to detect defects, breaks or other structural changes before they compromise the health of the entire construction.
In this type of sensing the optical fiber is embedded into or just put on the element to be inspected, like glued to steel bars of reinforced concrete before its pose or just laid on the surface of a material to not be affected by strain. The way the fiber is included in the desired structure is particularly important, since a wrong deployment could add errors in the acquired sensed data. For example, if the glue that keeps fixed the fiber onto a plate is bad, the fiber could not be strained in the same way the plate does, affecting the damage prediction and in the end maybe the stability of the structure. Moreover, during the pose it is necessary to be careful to adequately protect the fiber, in order to avoid future breaks that could be difficult to fix (as for a fiber embedded into reinforced concrete) [6].
The mechanism enabling the use of the fiber as a distributed sensor is the scattering of light. In order to explain this phenomenon however it is necessary to first consider how light propagates in an optical fiber. As it is well known, light can be guided within an optical fiber due to the so-called total internal reflection [7]. If a single mode fiber (SMF) is considered, where only one pulse of duration τ is launched, it is possible to know the spatial position z of the pulse thanks to the classic space-time relation $z = \frac{c}{n}t$, where c is the speed of light in vacuum, n is the refractive index of the medium (the core of the fiber) and t the time index. When however a reflection, like when light reaches the end of the fiber, or internal scattering occurs, part of the electromagnetic field can be guided backwards reaching the launch end. In this case, considering the previous equation, the reflected light from a particular position z_0 will reach the fiber front end at a time that is twice the one needed to reach z_0 from the launch, since light has to travel twice that

distance. So in this case, for the light that is going backwards, it is $z' = \frac{1}{2}\frac{c}{n}t'$ and in this way it is possible to detect spatial attributes of the fiber (defects, length, etc.) just by observing the time when light gets back at the fiber beginning.

The backscattered light that is then received is also dependent on the characteristics of the pulse that is launched into the fiber. A pulse of duration τ spatially occupies a portion of fiber that is $\Delta = \frac{c}{n}\tau$, moreover it affects the spatial resolution[1] that is possible to achieve with the photodetector. In fact, the received power at a certain time t is the sum of all contributions of the backscattered field that are originated in a part of the fiber of length $\Delta/2$, where the factor 2 is attributed to the travel time of incoming pumped and scattered light [8]. In this way, it can be said that launching a shorter pulse enables the detection of events, such as breaks or defects, that are smaller or closer to each other. It is however necessary to be said that the shorter the pulse the lower the SNR, due to the less power that is carried by the propagating pulse. It is also important to pay attention to the length of the fiber, since due to propagation losses it could be necessary to amplify the signal in order to receive sufficient backscattered power.

In case of fiber optics distributed sensors, the spatial resolution is related to the possibility of clearly detecting the differences on the spectrum of the backscattered light due to changes in strain and temperature: if the spatial resolution is increased, then more fiber points can be detected, thus increasing the accuracy of the sensor. Distributed sensors can be seen then as many point sensors, since due to the finite spatial resolution not the whole length of the fiber can be analyzed, so sometimes this light weight and low cost sensors (if only the optical fiber is considered) are better with respect to use many single point sensors.

[1]The spatial resolution is defined as the minimum distance between two events to be resolved.

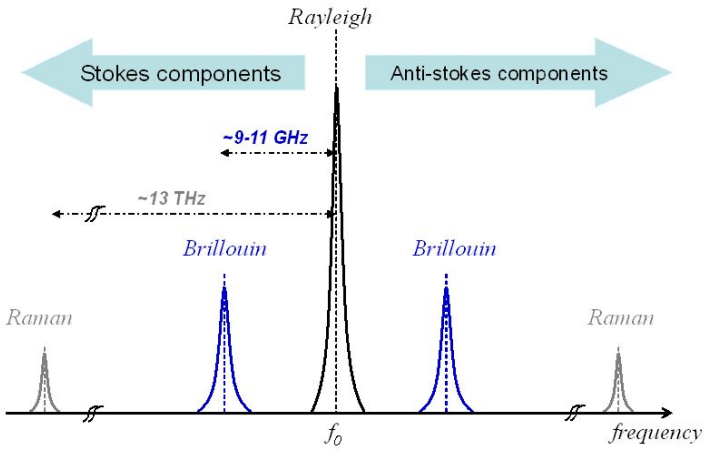

Figure 2.1: Scheme of the different spectra resulting from Rayleigh, Raman and Brillouin scattering processes in optical fibers [9].

2.1.1 Scattering effects

As previously commented, distributed optical fiber sensors are based on scattering processes that take place within the fiber. In general, a scattering process takes place when light goes through inhomogeneities of size much little than the propagating wavelength that scatter a little portion of light in all directions, reducing the propagating light power. If this reduction is proportional to the propagating power, the scattering is said to be linear, while it is called non-linear if the scattered power is not proportional to the original one. Scattering can also be elastic, if occurs without frequency shift, or inelastic, on the contrary. The inhomogeneities can be of many types, like microscopic or macroscopic variations in density, composition or structure of the material, which causes *Rayleigh* scattering. This is a linear and elastic scattering that causes an attenuation of the forward-propagating signal (and creation of a backward-propagating wave) proportional to $\frac{1}{\lambda^4}$. Molecular vibrations or optical phonons in the medium may also give rise to *Raman* scattering, a non-linear and inelastic process since the scattered wave is frequency shifted

of some THz. Sound waves or acoustic phonons give rise to the so-called *Brillouin* scattering, a non-linear and inelastic effect where the scatter occurs at some GHz of frequency shift. Figure 2.1 shows a schematic representation of the spectra associated with these processes, where the difference between Stokes and anti-Stokes components, i.e. down-shifted or up-shifted with respect to the propagating light, has also been considered.
All these types of scattering can occur in a spontaneous or stimulated manner. Generally, as long as the input light is scattered without strongly altering the properties of the medium, the scattering is considered spontaneous. When the light intensity increases to a level such that the optical properties of the medium are modified, and the scattered light is proportional to the power of the input light, then this regime becomes stimulated [8].

2.1.1.1 Rayleigh scattering

Rayleigh scattering is, as briefly mentioned before, the dominant scattering effect and loss mechanism in the low-absorption window between the ultraviolet and infrared absorption tails. The main cause of this effect are inhomogeneities of a random nature[2] occurring on a small scale compared with the wavelength of light[3] [7]. In general, the result of the presence of these inhomogeneities are refractive index fluctuations and the subsequent scattering, which occurs in almost all directions, giving an attenuation proportional to $\frac{1}{\lambda^4}$ following the Rayleigh scattering formula

$$\alpha_R = \frac{8\pi^3}{3\lambda^4} n^8 p^2 \beta_c k T_F,$$

where α_R is the Rayleigh scattering coefficient, λ the optical wavelength, n is the refractive index of the medium, p is the average photoelastic coefficient, β_c is the isothermal compressibility, k is the Boltzmann's constant and T_F

[2]Silica is a disordered material, so there are density and compositional variations on a microscopic scale, which are frozen into the glass lattice on cooling.

[3]Inhomogeneities of size comparable to the propagating wavelength give rise to Mie scattering.

is a fictive temperature or the glass transition temperature, representing the temperature at which the density fluctuations are "frozen" in the material, so when glass reaches thermal equilibrium. This relation can, for example, explain why the sky is blue: sun light is scattered in all directions when it enters in the atmosphere, due to gases and particles present in the air. Since the scattering is proportional to $\frac{1}{\lambda^4}$ however, blue light is the most scattered part of visible light thanks to its shorter wavelength with respect to the other colours of the rainbow.

Rayleigh scattering is a linear scattering, so the scattered power is proportional to the propagating one. However, since this scattering may occur in all directions, only a part of it can be backpropagated in the medium, being then useful for sensing purposes (especially when talking about optical fiber sensor systems). In fact, the fraction of captured optical power is $S = \frac{(NA)^2}{4n_{co}^2}$, where NA is the numerical aperture of the optical fiber and n_{co} is the refractive index of the core of the fiber. In this way, the backscattering coefficient is given by the product of the Rayleigh scattering coefficient and the fraction of the captured optical power.

Rayleigh scattering is the phenomenon enabling the (nowadays widespread) use of OTDRs (optical time domain reflectometer) and this, with the OFDR in the frequency domain, is also the main way to exploit Rayleigh (and also the other scattering processes) for sensing. In fact, the focus in these sections is on OTDR-based distributed sensors, where the previously explained space-time relation is exploited to characterize what is happening in the fiber by detecting the backscattered light, and specifically losses, in the time domain [10].

A typical OTDR trace is represented in Figure 2.2, where the most important loss effects are showed, however the important thing to be noticed is the relation with distance, thus allowing to detect where a given event is happening.

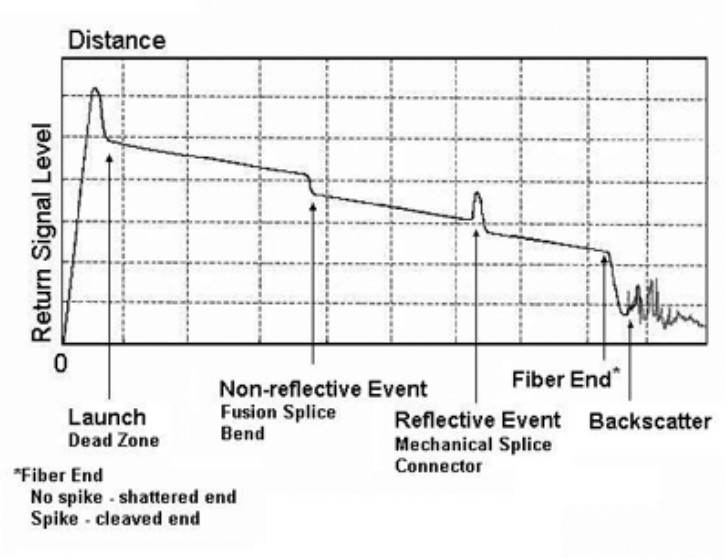

Figure 2.2: Typical trace of an OTDR, where the possible loss occurences in a fiber are showed [11].

There is however another approach, that is frequency-based, the so-called OFDR. In this case a tunable laser is used to scan a frequency range of ΔF and through Fourier transformation produces a spatial resolution of $\Delta = \frac{c}{2n\Delta F}$. While the sensing length in the OTDR systems is the fiber length, in the OFDR ones is limited by the coherence length of the laser source and the state of polarization change along the fiber. OFDR sensors tend to be sensitive to bending loss, so for civil structural monitoring, fibers must be protected from sharp bends and although OFDR often uses single mode fiber, it can also be implemented with multi-mode fiber [8].

2.1.1.2 Raman scattering

Raman scattering is a non-linear and inelastic process that occurs when an electromagnetic field (e.g. light) encounters an obstacle, periodically perturbing the matter molecules with the same frequency of the incident wave. This perturbation may be seen as a dipole, causing molecular excitement

and vibrations, that is also source of an EM field, thus a source of scattered light. If a quantum mechanics domain is considered, it can be said that if the photons of incident light have sufficient energy to be absorbed and change the energy level of the molecules (and its molecular vibration), there will be a remaining quantity of photon energy that exits from the molecules. This quantity can be considered as the scattered part of the light, with a different energy and so with a different oscillating frequency[4] [12]. As previously indicated, if the molecule is excited to a higher energy level the resulting scattering will be a Stokes wave, on the contrary if the molecule releases energy, lowering its energy, the scattered will be of the anti-Stokes type.
Raman scattering can be useful to sense temperature changes (but not strain) and a way is to excite both Stokes and anti-Stokes components, whose ratio depends on the temperature of the fiber. To exploit useful spontaneous Raman scattering it is however necessary to deliver into the fiber a high intensity optical pulse, since Raman is normally 20-30 dB lower than Rayleigh scattering. Another possibility is to use stimulated scattering, where it is necessary to have yet in the fiber photons with frequency equal to the scattered ones, in order to exploit a Raman gain [8]. In both cases the sensing is OTDR-based, so exploiting backscattering, however forward scattering can also be exploited, since Raman scattering can be excited both in co-propagating and counter-propagating configurations, where light is launched from the two ends of the fiber. This configuration gives less sensitivity but a higher signal level with respect to the back propagating one, even if it is normally necessary to have access to both ends of the fiber.

[4]Usually the frequency shift is about 1-10 THz (Figure 2.1).

2.2 Brillouin distributed sensing

Hereafter the main aspects of Brillouin distribute sensing will be explained, however it is worth noting that this document will not include many formulas and theoretical models for two main reasons: first for a simpler understanding for those not working in this field, second because there are many papers and reviews that have already carried out a great job on explaining the theoretical basis.

2.2.1 Brillouin scattering: spontaneous and SBS

As already discussed, this thesis is focused on Brillouin-based distributed sensing, therefore on Brillouin scattering. This is an inelastic and non-linear scattering caused by the propagation of density fluctuations of the medium resulting from propagating pressure waves. These pressure waves change periodically the refractive index as they propagate, thus they can be seen as moving Bragg gratings and the scattering then is through Bragg diffraction [13].
Light is scattered by acoustic waves with a frequency-shift that is dependent on the scattering angle. It is well known that for the Brillouin case the scattered light is propagated only in the backscattering direction, where its frequency shift is maximum following[5]

$$\nu_B = \frac{2nV_A}{\lambda_p}, \tag{2.1}$$

where n is the refractive index of the core, V_A is the sound velocity of the material and λ_p is the wavelength of the incident wave, called the *pump* wave. The backscattered wave is instead called *probe* wave. The sound velocity depends in turn on the waveguide material, in particular on its density. The scattering can also be seen as resulting from the Doppler effect, since the acoustic wave is moving inside the medium. Depending on its propagation

[5]Usually the frequency shift is about 11 GHz for monomode optical fiber (SMF) (Figure 2.1)

direction, the frequency of the scattered light is down-shifted (giving the Stokes component) when the acoustic wave is moving away from the incident light, while the frequency is up-shifted for the other case. As it takes some time for acoustic waves to fully build up (around 30 ns), the Brillouin line is normally $\Delta\nu_B \cong 30$ MHz.

Obviously, Brillouin scattering occurs under some precise conditions. In fact, there must be energy and momentum conservation between the waves that propagate in the medium (optical and acoustic); furthermore, the frequencies ν and the wavenumbers k must be such that[6]:

$$\nu_a = \nu_p - \nu_s \quad \text{Stokes case,} \qquad \nu_{as} = \nu_p + \nu_a \quad \text{anti-Stokes case} \tag{2.2}$$

$$k_a = k_p - k_s \quad \text{Stokes case,} \qquad k_{as} = k_p + k_a \quad \text{anti-Stokes case} \tag{2.3}$$

that constitute the typical energy and phase matching conditions of nonlinear interactions. All these conditions dictate backscattering of the incident light only by those acoustic waves whose frequency is in very close vicinity of ν_B, that is also called the *Brillouin Frequency Shift* (BFS) [1].

Regarding the Brillouin spectrum and linewidth, it can be demonstrated that the Brillouin scattered light exhibits a given linewidth due to attenuation of the acoustic wave involved in the process. The resulting spectrum, the so-called *Brillouin Gain Spectrum* (BGS) shows a Lorentzian spectral profile given by [14]:

$$g_B(\nu) = g_0 \frac{(\Delta\nu_B/2)^2}{(\nu - \nu_B)^2 + (\Delta\nu_B/2)^2}, \tag{2.4}$$

where $\Delta\nu_B$ is the full-width half-maximum (FWHM) (usually $\sim$30 MHz) and g_0 is the Brillouin peak at resonance ($\nu = \nu_B$).

Why Brillouin scattering is so important for distributed sensing? Differently from Raman scattering, Brillouin scattering and in particular the BFS is dependent from changes in both temperature and strain, so using appropriate investigation techniques it is possible to understand what is going on in the fiber. In general, for a standard SMF using 1550 nm wavelengths, the sensi-

[6] a is for *acoustic*, p is for *pump* or *incident* wave, s is for *Stokes* and *as* is for *anti-Stokes*

tivities are of 1 MHz per degree °C and of 50 MHz per 1000 με, i.e., 50 MHz per 0.1 % elongation/contraction of the fiber [1]. An example of how the BGS can change due to temperature or strain variations is reported in Figure 2.3. It is worth mentioning that, in addition, the BGS seems to exhibit a different behavior with strain and temperature. In particular, the associated linewidth (and peak intensity) varies in different ways, according if there is temperature or strain occurring onto the fiber [14]. This will be commented in detail in Chapter 5, where measurement results will be reported. As for Raman, Brillouin scattering can be spontaneous or stimulated, however it is also important to underline the differences between Brillouin and Raman Scattering. First of all, the frequency shift of the backscattered light with respect to the incident one: for Raman is about ten THz while for Brillouin is ten GHz. In addition, in optical fiber systems, Raman implementations can provide scattering in both directions (forward and backward), while Brillouin only generates a backscattered wave. Brillouin scattering is also 15-20 dB weaker than Rayleigh one, while Raman is 20-30 dB weaker [8].

2.2.1.1 Spontaneous scattering: BOTDR and BOFDR

Spontaneous scattering is caused by an incident light that is scattered by thermally initiated acoustic waves, i.e. acoustic phonons, creating both Stokes and anti-Stokes waves. They are down or up-shifted by the same frequency difference ν_B since it is dependent only on the sound velocity within the fiber. The acoustic phonons, that are pressure waves, act changing the dielectric permittivity since they are a periodical pattern (like a Bragg grating). They are assumed to be created by thermal agitation, so for any time $t > 0$ there will be a given (acoustic) phonon population within the fiber, thus giving rise to thermally generated acoustic waves (or energy) propagating through the fiber. These waves will be responsible for the scattering of the incoming pump (optical) wave, that, after this interaction, will travel

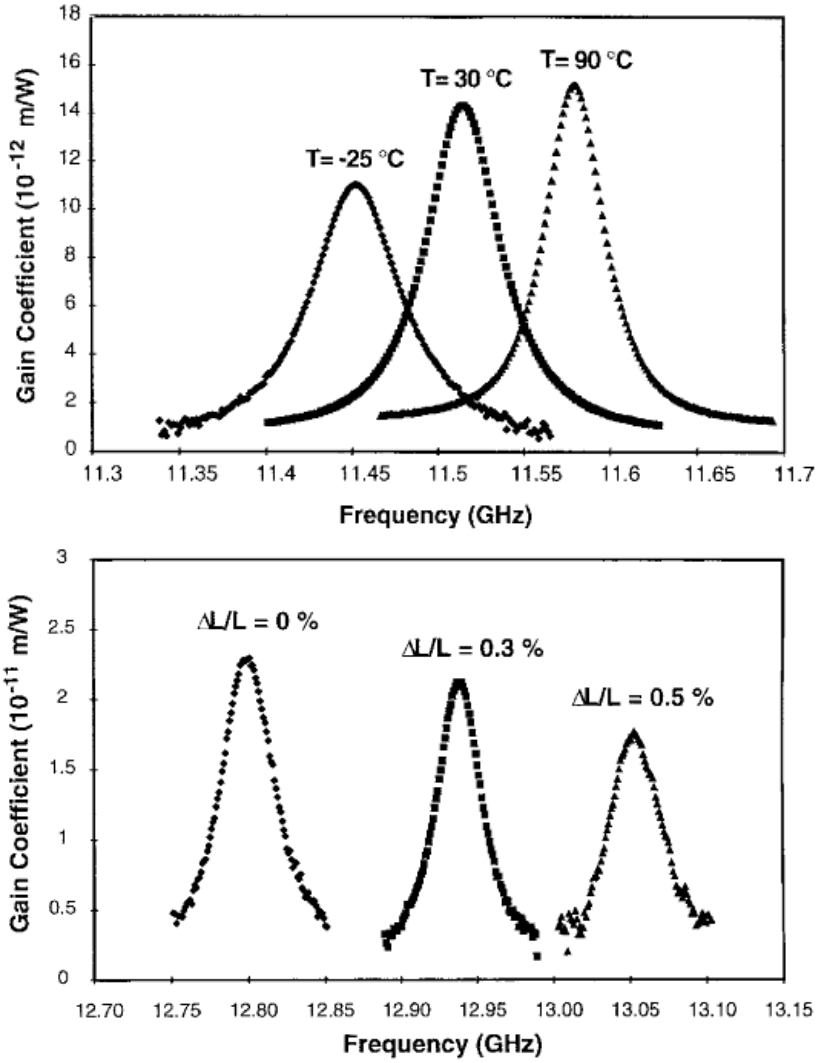

Figure 2.3: Example of different BGSs due to changes in temperature (on the top) and elongation (on the bottom) [14]. A difference in the behavior of the BGSs for temperature or strain increase is visible.

backwards with a given frequency shift (BFS) depending on the working wavelength and the chosen optical fiber. Practically, this can be seen as a power transfer from the input propagating light to another one, backpropagating, that happens to exist thanks to the scattering process.
The power of spontaneously scattered waves is normally weaker than the stimulated case and the backscattered wave should be properly amplified to be investigated, however the spontaneous case exhibits some interesting features, mainly the one-end access to the fiber under test (FUT) that allows to have simple yet powerful sensors. Depending on the proposed scheme, it is possible to develop the following implementations: Brillouin Optical Time Domain Reflectometry (BOTDR), Brillouin Optical Frequency Domain Reflectometry (BOFDR) or Brillouin Optical Correlation Domain Reflectometry (BOCDR). In this case attention will be dedicated only to BOTDR and BOFDR.

- BOTDR: this configuration shares the same basic working principle than an OTDR, based in this case on Brillouin scattering and not on Rayleigh effect. In this case a pulse of frequency ν_p and duration T is launched at one end of the fiber, $z = 0$. At a certain time t the backscattered wave, formed by both Stokes and anti-Stokes components, reach $z = 0$. This backscattered component is generated from a segment of length $\Delta z = V_g T/2$ at a distance $z' = V_g t/2$ where $V_g = \frac{c}{n}$ is the light speed in the fiber core. As said, Stokes and anti-Stokes wave are frequency shifted with respect to ν_p by the same absolute amount ν_B. This frequency deviation depends initially only on the chosen fiber and wavelength, but it exhibits a linear dependence with both strain and temperature at position z'. The backscattered signal could contain also Rayleigh, Raman or noise components, so it is important to filter out everything and usually it is partially done by selecting only the Stokes wave with, for example, a fiber Bragg grating (FBG). [1]
  The BFS can be retrieved in two ways: the first is to make interfere the

Stokes wave with the original pulse, in order to have both informations in frequency for a single point and also in distance. The maximum of each spectrum in each position z is $\nu_B(z)$, that is retrieved in the time domain thanks to a local microwave oscillator mixed with the electrical signal and then filtered with a narrow band filter. The second is to optically filter with a Mach-Zender Interferometer (MZI).
The major advantage of this configuration is that it is sufficient to have access only to one end of the fiber. However, the main issue here is the very low backscattered power, although it can be enhanced increasing the time of signal acquisition, the pulse power or the temporal averaging.

- BOFDR: it is an approach very similar to BOTDR, where again only one end of the fiber is needed to carry out the distributed measurement. In this case, the pulsed pump is substituted by a sinusoidally modulated continuous wave (CW) generated by a vector analyzer. The backscattered signal (also modulated) is detected (amplitude and phase) via the same vector analyzer. Finally, an inverse fast Fourier Transform is employed to retrieve the distributed information along the fiber.

2.2.1.2 Stimulated scattering: BOTDA, BOCDA and BOFDA

In stimulated Brillouin scattering (SBS), acoustic waves are induced by the pump wave that interferes with spontaneously scattered Stokes wave, thanks to a phenomenon called electrostriction, that is the tendency of dielectric materials to become compressed in presence of an electric field. This phenomenon causes a pressure wave which changes periodically the refractive index, thus acting like an acoustic wave.
As explained, the adjective *stimulated* is related to the fact that only if the input power is high enough there will be the presence of acoustic phonons, and so acoustic waves, that will let the pump wave exchange with the backscattered one more power with respect to the spontaneous case. In fact, the

interaction between the pump and the acoustic wave, which propagate in the same direction, gives rise to a backscattered Stokes wave according to the energy and phase matching conditions described in (2.2) and (2.3). This Stokes wave in turn reinforces the acoustic wave, that acts as a Bragg grating scattering a higher part of incident light [15].
There is however another way to exploit stimulated Brillouin scattering, as reported in [1]. In this case it is necessary to have access to both ends of the fiber since both pump and probe waves are given as input with a frequency difference $\nu_a = \nu_p - \nu_s$, where the probe wave acts as the Stokes wave. Their interference, thanks to electrostriction, gives rise to a density wave that is at its maximum only when $\frac{2\pi\nu_a}{k_a} = V_A$ that is the dispersion relation of acoustic waves in the fiber, so when $\nu_a = \nu_B$. Therefore when their frequency difference is close to the BFS, there is the maximum power exchange from the pump to the probe, obtaining in this way a gain, the BGS, for the Stokes wave. This gain depends on the acoustic wave so, as before, it has Lorentzian shape and a linewidth of about 30 MHz.
Clearly, the required access to both ends of the fiber is an issue and a disadvantage in comparison to the spontaneous case, however here it is possible to obtain higher backscattered waves, thus easier to be examined.
As the spontaneous case, the stimulated Brillouin scattering is exploited for many different configurations such as Brillouin Optical Time Domain Analysis (BOTDA), Brillouin Optical Frequency Domain Analysis (BOFDA), Brillouin Optical Correlation Domain Analysis (BOCDA) and others. Here they will be briefly reported and explained, with the exception of the BOTDA case, which will be thoroughly revised in a following section. In general all these informations are reported in [1], however the first papers where these configurations have been explained will be cited.

- BOFDA: here two narrow-linewidth lasers (or a single one that can be coupled to give to lightwaves) are respectively coupled in the two ends of the fiber, where the probe frequency is downshifted with respect to

the pump one of a quantity equal to the characteristic BFS. The probe is then modulated in amplitude with a variable angular modulation frequency and, for each value, the alternate components of the pump and the probe intensity are registered at the end of the fiber. The loss of the pump is registered and used to recover the baseband transfer function of the fiber, then digitized and fed to a processor who gives as output the inverse fast Fourier transform (IFFT) that looks like the distribution of temperature and strain along the fiber. [16]

- BOCDA: this configuration is used to perform dynamic measurements and it is based on the correlation between the pump and the probe which excite SBS. The measurement is performed controlling the coherence between pump and probe, sinusoidally modulated, in order to have a stable acoustic field only in predetermined positions. If the pump and the probe are modulated by the same waveform, the pump-probe beat spectrum will be like a delta function, so the SBS will be present only where there is high correlation between them. Varying the pump-probe mean frequency difference, the gain of the probe at the peak correlation point varies according to the BGS. In any case, it is possible to obtain the BFS just by scanning the difference between pump and probe frequency where the correlation is high and look to its maximum [17].

- Other configurations - BDG: the mentioned configurations are only few and the earliest versions of a bigger amount of methods and ways to exploit Brillouin scattering in optical fibers as sensors. Besides simplifications or modifications of the above schemes, there can be also Brillouin dynamic gratings (BDG) where a pump and a probe having the same polarization interferes building an acoustic wave, which behaves like a Bragg grating, in a polarization maintaining (PM) fiber. In this case, it is possible to scatter another couple of waves, orthogonally

polarized with respect to the previous ones, that act as interrogators of the fiber. The BGS and so the BFS can be retrieved by sweeping the frequency difference between pump and probe, however it can give a higher spatial resolution with respect to the BOTDA configurations, for example as reported in [18].

2.2.2 BOTDA

BOTDA is the most common Brillouin interrogation technique and also the one used in this thesis. It is based upon the counter-propagation of two waves: a pulsed pump wave and a continuous wave (CW) probe, launched respectively at $z = 0$ and $z = L$[7], where L is the FUT length. The probe frequency ν_{probe} is lower than the pump one ν_{pulse} and, thanks to the electrostriction, where their interaction takes place they give rise to a density wave, i.e. an acoustic wave whose frequency is $\nu_a = \nu_{pump} - \nu_{probe}$, which scatters the pump wave giving gain to the probe, depending on how much ν_a is close to the BFS. The BGS is then obtainable sweeping the probe or pump frequency, in order to change their frequency difference in a proper range, thus detecting the probe wave at $z = 0$. It is also possible to have the contrary, having a CW pump and a pulsed probe, thus measuring the loss and not the gain of the probe wave.
The general scheme of a BOTDA setup is reported in Figure 2.4. A narrowband laser (usually of ∼1550 nm) is splitted, using an optical coupler of the appropriate coupling ratio, into two lightwaves that are the starting points to generate the pulsed pump and the CW probe. The upper branch shows the pump generation scheme, where the lightwave is intensity modulated by a device that shapes the signal as a pulse by using an electro-optical modulator (EOM), a semiconductor optical amplifier (SOA) or another modulating device with high extinction ratio in order to do not have signal where it is

[7]It is then necessary to have access to both ends of the fiber.

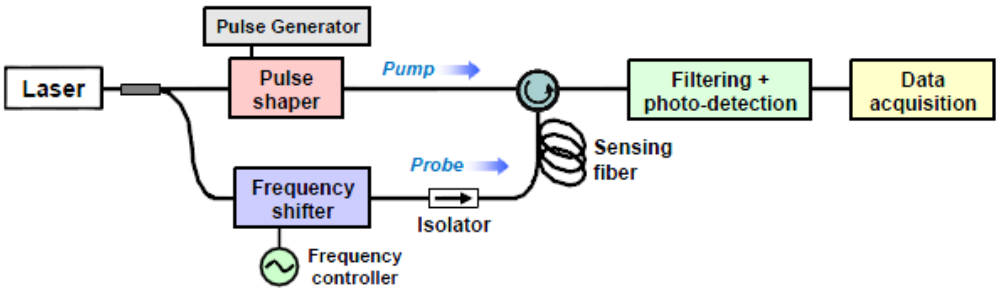

Figure 2.4: General setup scheme for a BOTDA configuration [2].

unwanted. This pulse is then repeated with a certain frequency and with given intensity by the pulse generator and eventually optically amplified, thus entering one end of the FUT. The lower branch indicates instead the generation process of the CW probe: this is made using an optical frequency shifting device, in which the frequency shift between the pump and the probe can be precisely controlled. Usually an EOM driven by a microwave signal is employed, in order to generate a double-sideband suppressed carrier CW probe wave. After going through an isolator, to do not let the pump exits the FUT, this signal is launched into the other end of the FUT, where interferes with the pump giving rise to the scattering process. The light resulting from one of the sidebands is then filtered out and the scattered lightwave is detected by a photodetector [2].

This general scheme however does not account for some critical issues that may occur using this configuration, which are important to consider in order to effectively excite SBS and use it for sensing purposes. Moreover, it is nice to explain why some devices and some precautions are used. Hereafter some of the most significant problems will be listed and briefly explained, since they have an impact on the setup and on the values of some parameters. Some of them are reported in [1], [2], [8], etc.

- **Spatial resolution**: this is one of the most important features of the configuration, since it specifies the minimum distance between two points that can be effectively resolved by the sensor system. As ex-

plained in the first subsection of this chapter, the spatial resolution is $\Delta z = \frac{1}{2}\frac{c}{n}\tau$ where τ is the time duration of the pulsed pump, so it would be better to have a very short pulse in order to have a high spatial resolution. In this way the SNR is lower with higher spatial resolutions, since the pump pulse carries less optical power, however there is another BOTDA specific problem due to too short pulses. In fact, it takes ∼30 ns to fully build up the acoustic wave (i.e. to reach the 99% of its maximum) thanks to the interference of the pump and the probe, so a pulse shorter than that would broaden the spectrum, making it difficult to identify the peak of the BGS that is associated with the BFS. For this reason,the maximum spatial resolution that can be achieved via a conventional BOTDA implementation is ∼1 m.

- **Polarization fading**: this issue is related to the fact that usually BOTDA is used over common SMFs and not on PM ones, so the parallelism between the states of polarization (SOPs) of the pump and the probe can not be maintained. Their polarizations, duo to a weak birefringence of the fiber, change while propagating in the fiber, thus it is possible to have minimums and maximums of interaction between them that compromise the homogeneity of the gain. In order to solve this problem a polarization scrambler, a polarization switch or other methods that can randomize or stabilize the polarization of the propagating waves can be used, placed in the pump and/or probe arm.

- **Pump depletion**: this is another issue related to the generation of a non-homogeneous gain. It is known that the higher is the pump, the higher will be its interaction with the probe and consequently their power exchange. It is immediate to understand, however, that if the pump loses too much power during its propagation in the fiber, at a certain point it will not have enough power to excite SBS, quenching the gain and affecting the evaluation of the BFS over the whole fiber

length. This can be dealt with by means of different strategies, for example working in a small gain regime [2] or using an electro-optical modulator (EOM) of the Mach-Zender type, working at its zero transmission point, driven by a microwave signal to generate two sidebands of a sine wave. Only the lower sideband will be used as probe, however the upper one will be discarded only right before the detection since it is useful as it exchange its power with the pump, that was weakened by the lower sideband. Since the two sidebands are frequency shifted by the same absolute value with respect to the pump wave, it is possible to avoid pump losses of power [14].

The maximum sensing length depends on the FUT, on the pump power and consequently on the spatial resolution. If a high spatial resolution is needed, a lower distance can be reached (in a conventional BOTDA setup) since the pump pulse will have a very low power and it will be attenuated soon by the fiber.

It is also important considering the possibility of having errors in the evaluation of the BFS. It could be due to an erroneous setup (yielding the above mentioned problems), due to the presence of noise added to the useful signal or due to low spatial/frequency resolution. The error can then be generally reduced taking more than one trace for the same frequency difference and performing an averaging. In this way, the detector can receive a higher amount of traces, lowering the noise and increasing the SNR. In fact the number of averaged traces N_{AV} impacts on the frequency error (BFS estimation) by reducing it by a factor proportional to $1/\sqrt{N_{AV}}$ [2].

Once the basics regarding BOTDA sensors have been considered, the following section will be devoted to the problem where this thesis is focused on: the discrimination between strain and temperature in BOTDA measurements.

2.3 Discrimination between strain and temperature in BOTDA setups

In section 2.2.1 (and Figure 2.3) it was reported that the Brillouin scattering is dependent on changes in temperature or strain (could it be elongation, stress, bending, twist, etc.) that affects the fiber. Each of these parameters has a different impact on the dielectric, thus on the behavior of the scattering process and of the resulting BGS. However, if both are occurring at the same time and in the same position, the overall result is a frequency shift, a change in the width and in the gain peak that could be in fact the outcome of many different temperature/strain combinations. If then the fiber must be an accurate sensor, understanding what is going on is fundamental: if the sensor is supposed to be fixed to something but needs to sense fire or particular temperature differences (for example, on far high-voltage power lines), it is important to distinguish and discriminate between the two, to do not alarm technicians in vain in such a case.
The discrimination between the effect of strain and temperature in a fiber, using BOTDA configurations, is also the objective of this thesis. Here some of the discrimination methods known in the literature will be reported, from the simplest to the BOTDA ones, also going through other types of scattering or Brillouin configurations.
The simplest way to discriminate strain and temperature is to have separated methods to sense different combinations of the two effects. One of the methods could be using the same configuration, for example BOTDA, where one section of the fiber is bounded to the object under sensing (thus sensing both temperature and strain) and the other is just leant on it (sensing only temperature). Another way is to use Raman scattering to sense only temperature and then exploiting Brillouin sensing to sense both, in order to distinguish and separate the effect of temperature and strain on the frequency shift, since it has a linear dependence with them. Following this path, it can

be possible also working with both Brillouin and Rayleigh scattering as two independent measurements, combining then the results. Other articles reports also to use FBG for local strain measurement and distributed Brillouin sensing for both, to acquire temperature informations.
It is clear that having two unknown parameters, such as the temperature and the strain that are occurring to the fiber, it is useful to have two independent measurements or features that depends on the two quantities in different ways and with different relations. For example, another method of this type is based on spontaneous or stimulated scatterings and the acquisition of both frequency shift and peak power of the BGS, measuring the gain or the loss of the signal. As seen in Figure 2.3, both strain and temperature have an effect on the frequency shift (in an analogous way) and on the maximum gain (with an inverse behavior). Similar to this procedure, in other papers researchers have demonstrated the possibility to measure the BFS and the fiber birefringence, or BFS and power loss/gain and the bandwidth of the BGS in PM fibers.
Other possibility is to use suitable cables, existent or specifically built, and exploit their customized characteristics (for example, to have more than one Brillouin peak) in order to have independent measurement quantities (LEAF fiber).
In this thesis the goal is to discriminate strain and temperature in a BOTDA setup using artificial neural networks (ANNs), given that this would be the first time to our knowledge that such approach is explored. In 1998 Chan et al. paper [19] an ANN approach is used, with good results, however they used simulations and not real measurements as data inputs. In this case data are retrieved in the laboratory and the whole process of measurements and post processing will be here illustrated, after the following chapter which will be focused on what ANNs are, how they work and why they were chosen for this discrimination goal.

3

Artificial Neural Networks - ANNs

Digital computation is nowadays the most powerful and fast tool we have to perform many difficult, long and iterative tasks. Also, the same tasks would take too much time, or also could be never solved, by a normal human brain. However our brain is still the most fast and precise tool when the task is about recognizing a pattern, such as a sound or an image.
For these reasons machine learning systems were developed starting in the mid 20th century (with theoretical studies) and keeping improving nowadays, with several different paradigms such as artificial neural networks, which try to mimic the behavior of the human brain in an attempt to solve specific tasks or problems.
The purpose of this chapter is therefore to put some light on this really powerful yet complicated tool, since it will be the one used to try to discriminate the effect of strain and temperature in a silica optical fiber.

3.1 What

The human brain is a complex structure with high parallelism that can be however represented by few functional units. It gathers billions of neurons interconnected by dendrites and axons which share informations through the synapses with the cell body and its nucleus [20]. The synapse, depending on the received signal, releases a neurotransmitter signal that forces the neuron to which is directed to produce a new electrical signal, if it is over the neuron threshold.

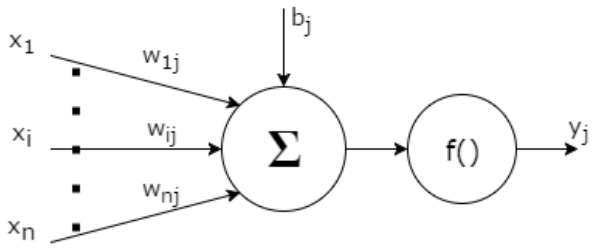

Figure 3.1: General ANN unit, j.

In order to succeed to reproduce this kind of communication and functioning, based on thresholds and many connections between the cell neurons, a mathematical model was developed starting between the 80s and the 90s: each neural network is represented by a number n of neurons (as the brain) that are interconnected by connections that represent axons and dendrites. Each connection has a weight w that symbolizes the role of the synapse that shares infos with a neuron with threshold of b.
Using this notation, the output of a single neuron j, which is receiving signals x_i from a neuron i that is connected with weight w_{ij} to j, is

$$y_j = f\left(\sum_{i=1}^{n} x_i w_{ij} - b_j\right), \forall j \in n. \tag{3.1}$$

A scheme of how a neuron works is reported in Figure 3.1. Weights can be positive if the connection excites the neurons, while negative if the connection inhibits the neuron to which is connected. If a neuron i is not connected to j, then $w_{ij} = 0$, while f is called activation function, which represents the firing intensity of the neuron. The activation function is a nonlinear function that transforms the linear combination of the input into the output, while the most commonly used functions are linear, ramp, step and sigmoid functions, as reported in Figure 3.2.
Neuron units in ANNs are arranged in layers, just as neurons in human brain are arranged in groups dedicated to different functions, and they can be from

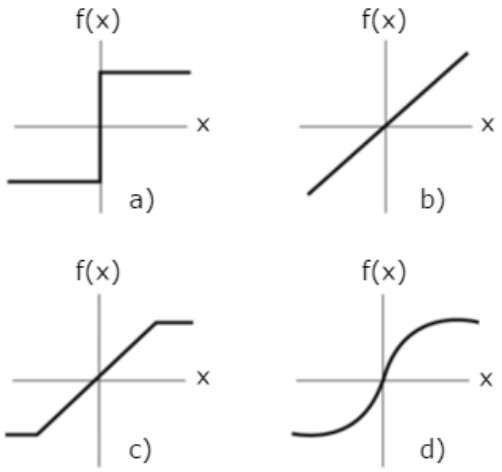

Figure 3.2: Different activation functions: a) step, b) linear, c) ramp, d) sigmoid.

few to many, depending on the desired behavior and the difficulty of the required task. Data are given as input to the neural network via the *input layer*, go through one or more *hidden layers* that assure the ability to solve nonlinear problems, and exit by the *output layer*. A network with more than one layer is also called *Multi Layer Perceptron* (MLP). Obviously, neuron units could never be as much as the neurons of the human brain, thus the achieved complexity is still lower.

The basic concept about working with artificial neural networks is their ability to learn from examples. In fact, an ANN works in two major steps: the first is the *training* phase, while the second is the *validation and test* one. In the first, input pairs of input and desired outputs are given to the ANN, that depending on the learning algorithm changes its weights in order to have outcomes that are as close as possible to the real, desired ones. Once the ANN is built, if for simplicity the validation step is not considered and left for a later explanation, the test phase can start, where only input data is given to the network. If the training is properly done, the outcome of the network is the correct one with a high percentage (classification rate).

Neural networks can be of many types, depending on: their function, the degree of connectivity between the neurons and the direction of the flow of the informations (topology) and the learning strategies; also, their general characteristics, such as nonlinearity, high parallelism, robustness, fault and failure tolerance, learning, ability to handle imprecise and fuzzy information, and their capability to generalize, make them an appealing tool for many different applications [20].

3.2 How

The most important phase when working with ANNs is the training one, because it determines how good the results will be. Depending on the topology and on the learning mechanics of the artificial network, its result can change a lot, so a proper choice of the network will be essential for a properly solved task.
Hereafter a brief review of the main used approaches will be done.

3.2.1 Topology: feedforward and feedback networks

In this type of scenario, the word *topology* indicates not only how neurons are connected together, arranged in layers, or about how many they are, but is strictly related also to how the learning algorithm behaves exploiting the network architecture.
Connections can me made from units of a layer to units of the following one, called *interlayer* connections, or also from units of a layer to units of the same one, called *intralayer* connections. It is also possible to have both types [21]. Also, the degree of connectivity tells if each neuron of a layer is connected to each neuron of the following one (full) or if some connections are missing (partial).

Depending on these connections, the neural network can be of the *feedforward* or *feedback* type:

- **Feedforward**: in this type of network connections never do cycles or loops, so there are only interlayer connections. In this case, depending on the learning algorithm, the error is calculated only once the initial data passed through each layer reaching the end of the network. The most used learning mechanism for this topology is the *backpropagation* (BP) algorithm.

- **Feedback**: in these networks, called also recurrent networks, outputs of some neurons are fed back to the same neurons or to neurons in preceding layers. This enables the network to exhibit dynamic temporal behavior and use it as a dynamic memory. This allows the network to perform its task not only looking at the single input-output pair, but also (eventually) to the following ones [20].

The learning strategy can be of two types: *supervised* or *unsupervised* learning (in [21] examples of both are found):

- **Supervised**: in this learning type an ANN is trained with the correct target outputs given with every input example, then using the deviation (error) of the ANN output from corresponding target values to determine the required amount by which each weight should be adjusted. A supervised learning ANN is also the one reported in Section 3.1 where the basic concepts were explained, since it is easier to have better results if the correct answer is known.

- **Unsupervised**: in this case it is possible to give as training only input data without the corresponding correct target; exploring the underlying structure in the data and the correlation between the various examples, the ANN organizes the examples into clusters (categories) based on their similarity or dissimilarity.

3.2.2 Feedforward network with backpropagation algorithm

The most common and simple feedforward network uses the BP algorithm for the training phase. A backpropagation network consists in a MLP of: an input layer that represents the input variables of the problem, an output layer that represents the correspondent output variables, one or more hidden layers that help modeling the nonlinearity of the problem. In this thesis a supervised learning will be exploited, so the ANN works by examples.
The backpropagation algorithm works in this way: the error that is computed at the output layer using gradient descent (or other optimization algorithms[1]), is then backpropagated from output to input layer in order to adjust ANN weights [20, 21]. The weights adjustment is performed until the error at the output is low enough, where *enough* is dictated by the task.

Up to this point ANNs were reported to have only two phases, the training and the test ones. However, it is necessary to talk about a problem that could occur when training an ANN. The complexity of the task could take the user to build a neural network with a lot of neurons or more than one hidden layer, in order to have as much freedom as possible to solve the problem. If however the ANN is oversized, there could be a problem of data overfitting: if this happens, it is possible that the network is not learning from examples, being then able to generalize in case of new inputs in the test phase, but it is just memorizing input-target pairs, giving then a wrong result when the network is tested with different data.
For this reason, between training and test phases, there is an intermediate one called *validation* phase: here a part of the input data, different from the training or test one, is selected and given to the ANN right after the training phase, to see if the error is high or not. Until the error is not acceptable, the training still goes on.

[1]Many different algorithms are developed, they can be more or less fast and require more or less memory.

3.3 Why

As just reported, since ANNs can be of many different types, it is possible to agree on the vast amount of tasks that neural networks can face. ANNs can perform prediction, forecasting, classification, pattern recognition, data processing, error compensation and many others. They also apply to different fields: economics, biology, mathematics, science, engineering, medicine, energy, sport and whatever needs nonlinear tasks to be solved.
At the end of Section 3.1 a list of the main characteristics of an ANN was reported; now it is useful to understand why those features are so appealing: nonlinearity allows better fit to the data, noise-insensitivity provides accurate prediction in the presence of uncertain data and measurement errors, high parallelism implies fast processing and hardware failure-tolerance, learning and adaptivity allow the system to modify its internal structure in response to changing environments, and generalization enables application of the model to unlearned data [20].

3.3.1 Application to photonics and distributed optical fiber sensors

ANNs will be used in this thesis to try to discriminate the effect of strain and temperature in distributed optical fiber sensors. Even if ANNs are useful also to biological systems, soccer patterns or also other odd things, it is quite interesting to see how they behaved for other tasks in the same field, also to justify its use in this case.
In [22] a neural network is applied to process the BOTDA trace in order to extract the temperature information along the fiber after the data acquisition. The results showed that the ANN provides higher accuracy and larger tolerance to measurement errors than Lorentzian curve fitting does, especially for a large frequency scanning step. Hence the measurement time can be greatly reduced by adopting a larger frequency scanning step without

sacrificing accuracy.
In [23] a discrimination between temperature and strain is proposed in case of an FBG, where two of them are embedded into the sensing fiber. Their different behavior and change in wavelength is useful since the two unknown parameters can be recovered with two independent amounts; ANNs here are used instead of the classic matrix approach to reduce the classification error. Many other papers use ANNs to classify and identify data, combined with other processing methods, in the field of Photonics, such as in [24] or [25], however the attention here will be all given to the discrimination process as discussed in [19].
In the following section the use of ANN for this thesis will be explained, even if it will be done after a proper discussion over the setup exploited for the measurements.

4

Experimental setup

Once all the theoretical bases have been reported, it is possible to start talking about the procedures and methods used to reach the goal. To do so, it is necessary to have a system that allows to physically perform the measurements (which comprehends laser, optical fiber, photodiode, etc.), some tools or setups enabling the presence of suitable conditions to perform them (i.e. a setup allowing to change temperature and/or strain conditions of the fiber) and something, specifically a software/computing tool, that bear an appropriate post processing of measured data.
Therefore, in this chapter all the tools, setups and configurations that have been used in this thesis will be analyzed and explained, in a chronological-like order, from measurement to post processing and final decisions. It is required to say that all these instruments were yet present or built on purpose thanks to and in the Photonic Engineering Group at University of Cantabria in Santander, Spain.

4.1 Experimental measurements

4.1.1 BOTDA configuration

The BOTDA setup used for the experimental tests is the same as the one reported in Section 2.2.2. In Figure 4.1 a more precise and detailed scheme is represented, thus a brief review of the configuration will be here done, adding

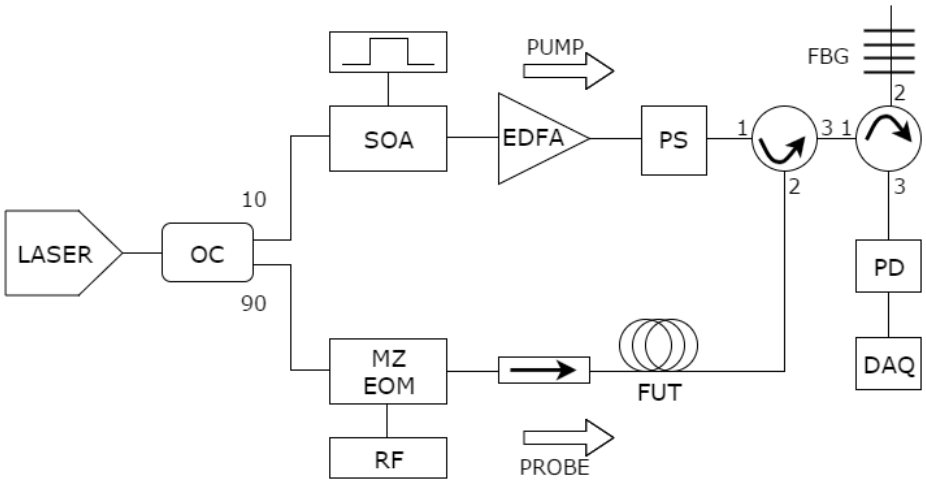

Figure 4.1: Schematic setup of the BOTDA system used in the experimental tests: Optical Coupler (OC), Semiconductor Optical Amplifier (SOA), Erbium Doped Fiber Amplifier (EDFA), Polarization Scrambler (PS), Mach-Zender Electro-Optical Modulator (MZ-EOM), RF Generator (RF), Fiber Under Test (FUT), Fiber Bragg Grating (FBG), Photodetector (PD) and Acquisition Card (DAQ).

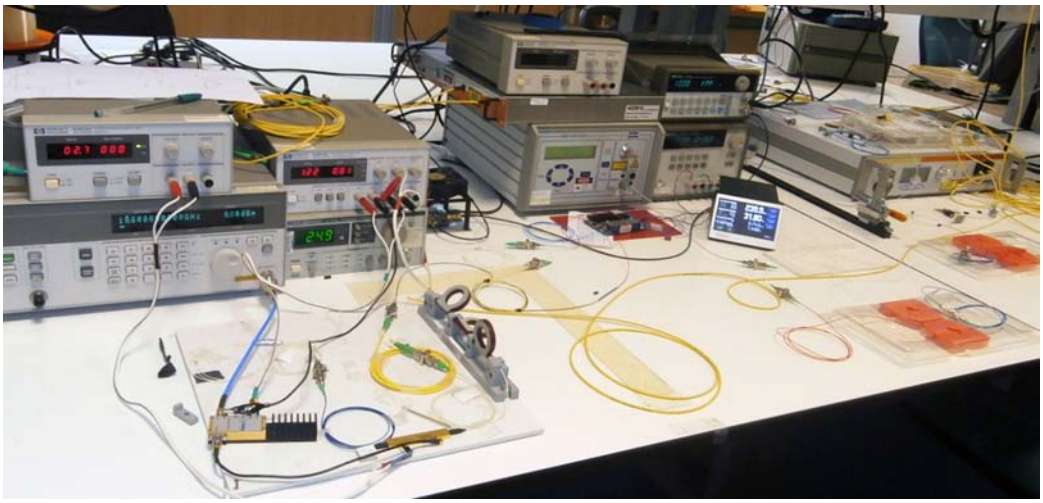

Figure 4.2: Physical implementation of the BOTDA scheme.

some technical characteristics of the working devices.
A single LD source (λ = 1550.92 nm) generates the light required for both pulsed pump and CW probe waves. The 90/10 optical coupler located at the output of the laser source divides the light (10% to the pump wave, 90% to the probe wave) into the two branches. The upper one generates the pump pulse long about 12 ns via a semiconductor optical amplifier (SOA), while the pulse generator was chosen to generate rectangular pulses of desired amplitude and frequency. The pump pulse is amplified via an erbium doped fiber amplifier (EDFA), whose gain is adjusted to have sufficiently Brillouin gain but not too much to do not have pump depletion. A polarization scrambler is then employed in the pump branch to avoid the polarization dependence of the SBS gain along the fiber and have an homogeneous pump-probe interaction. The probe wave is generated by an EOM that is fed by a RF generator that provides a sine wave, thus giving rise to two sidebands and a carrier that is suppressed by adjusting the bias voltage of the EOM (bias set 1at the zero transmission point). Both sidebands are transmitted via an optical isolator to the FUT, where they will interact with the pump pulse giving rise to stimulated Brillouin scattering, that will be then sent to port three of the first optical circulator to be detected. The second circulator allows to select the lower frequency sideband with a FBG, the signal then goes through a high-transimpedance gain 125 MHz photodetector (PD) and acquisition card (DAQ) integrated in a PC. In Figure 4.2 the physical implementation of this BOTDA configuration is represented.

4.1.1.1 Data acquisition

The data acquisition card consists in an oscilloscope which measures the electrical signal produced by the PD. Thanks to the Photonic Engineering Group in Santander, Spain, where this thesis has been done, it was possible to use an appropriate MATLAB® script in order to better control the measure-

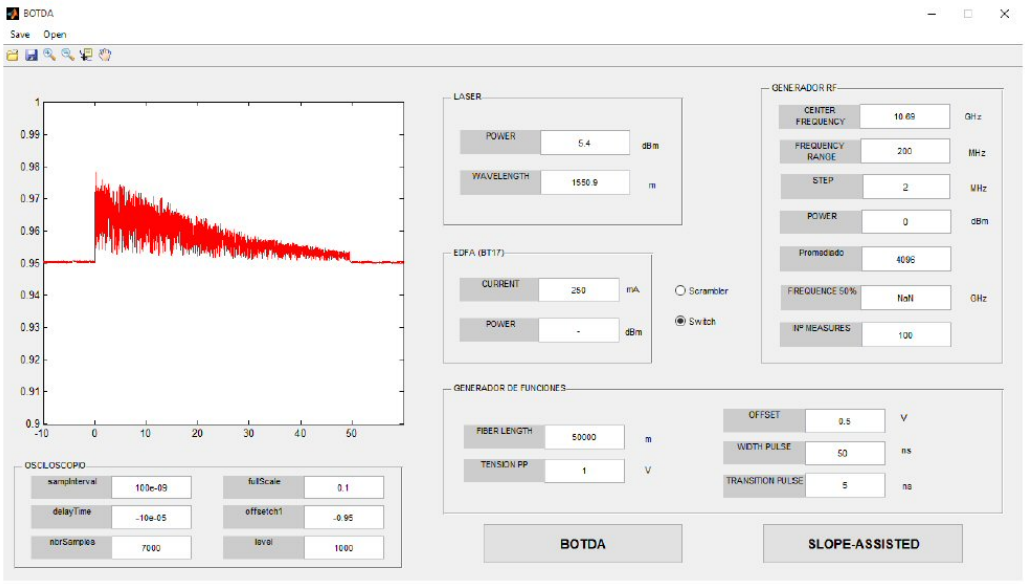

Figure 4.3: Only the "osciloscopio" and "generador de RF" sections were used, where the others are useful to other types of measurement. At the top left an example of how BOTDA trace should be is reported.

ment and the data acquisition. An interface of immediate understanding, reported in Figure 4.3, is made to handle the frequency sweeping between the pump and the probe (i.e. changing the probe frequency), thus to select the frequency range and frequency step used for the measurements and other oscilloscope characteristics like the averaging number, the sampling interval and the number of acquired samples. A quasi-real time Brillouin trace is also displayed, in order to let easily adjust the setup or the acquisition parameters if an unsuitable signal is detected. Once the acquisition is finished, the gain is automatically determined by dividing the signal by the probe output power before launching the pump wave (trying to avoid the negative contribution from a possible pump leakage) and then, scanning the required range of the pump-probe frequency difference, the normalized BGS along the whole fiber is reconstructed.

4.1.2 Temperature and strain changing tools

This thesis work required a long developing time and different phases in order to reach the final purpose: first, the focus was to take confidence with the BOTDA setup, the measurements and the post processing tool (ANNs), changing only the temperature of the fiber. The second was to implement a specific setup to strain in a restrained manner the fiber and the third was to create a controllable system that could enable to change both temperature and strain on the fiber at the same time.
Hereafter, a view on the physical instrumentations and setups used for the required experimental tests will be done.

4.1.2.1 Temperature measurements

To perform the initial temperature measurements, an already present climatic chamber was used (see Figure 4.4). A segment of the FUT, rolled as a spool, was placed inside the chamber, while the remaining fiber (and BOTDA setup) was connected to it in order to register the distributed measurements under temperature changes.

4.1.2.2 Strain measurements

For the second objective, a customized system was implemented to strain the fiber in a controlled and ideally homogeneous way. This was composed by two plastic wheels, distant $\sim$1.5 m, with a rough groove in the middle to keep the fiber restrained (see Figure 4.5). One (on the right of the picture) was screwed on the table to keep the fiber blocked at one side, while the other (on the left) was screwed on another support that, thanks to a spring and a reel, is able to pull the fiber by a desired amount (detail in Figure 4.6). In Figure 4.5, it is possible to see that in the middle of the table there is also a little metal plate whose function is to keep the fiber blocked and do not let it slip when strain is applied. In fact, two fiber coils are used: the part of

Figure 4.4: Picture of the climatic chamber used for temperature only measurements.

fiber to be stressed (some tens of meters) is retrieved from one end of one of the coils, bounded and rolled up onto the system to make some rounds and then fuse it to one end of the other fiber. In this way the strained part is in the middle of the acquired trace. The metal plate fixes the very end of the stressed fiber where it returns to the coils, after the fusion, in order to stress only that specific fiber part and trying not to modify the fiber positioning when strain is applied.

Figure 4.5: Picture of the strain measurement setup: it is possible to notice two fiber coils, the plastic wheels (1 the movable, 2 the fixed) and the fiber positioned in between. 3 is the metal plate.

Figure 4.6: Picture of the reel put under the plastic wheel in order to move it and strain the fiber leant on it.

4.1.2.3 Temperature and strain measurements

In order to simultaneously change the temperature and strain affecting the FUT the above reported tools are not suitable: the climatic chamber is too

little to support the strain-specific setup and, of course, it would be impossible to change the temperature of the room in a controlled and uniform manner.
One of the easiest and most common ways to obtain an homogeneous temperature distribution is to use water, that thanks to its properties can be used to uniformly heat objects inside it. For this reason it was necessary to build a customized system to heat water and in which it could be possible to insert a strain changer. The strain modifier was implemented in a similar way as the previous one and it is showed in Figure 4.7.

Figure 4.7: Strain modifier: at the ends of the aluminum bar there are the two black plastic wheels (to the left the movable, to the right the fixed) with fiber around them, in between two metal plates to fix the FUT.

Two plastic circles, adequately modified to properly hold the fiber around them, are fixed to an aluminum bar at a distance of 1.33 m each other. As before, two metal plates block both ends of the fiber (which is kept onto the system as before) in order to do not let it slip away when strain is applied. A detail of the plate is reported in Figure 4.8, where not only the fiber is visible (the upper two) but also another couple of fibers, that correspond to an FBG placed in the same way as the fiber in order to have another reference for the real strain value.
Figure 4.9 represents a detail of one wheel and how the fiber is rolled up on it. The way the fiber is not overlying itself, while doing circles around the system, is really important for the strain to be as homogeneous as possible. This behavior will be commented later in the following chapter.

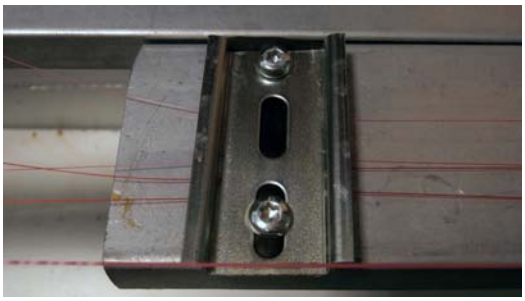

Figure 4.8: Detail of one of the blocking metal plates. Four fibers are visible passing under it, which are the two ends of the sensing fiber and the FBG.

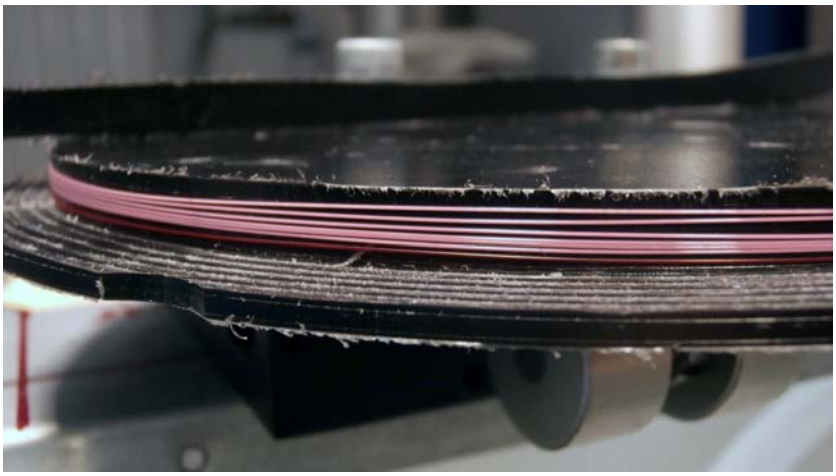

Figure 4.9: Detail of one of the two wheels with seven turns of the FUT around the system and the FBG at the bottom. In this case, fiber is not overlapping itself.

This portable system can be inserted in a 142×32 cm (length× width) aluminum tank, coated with insulating polystyrene, whose function is to contain the water to be heated and change the temperature of the fiber. In this regard, it was necessary to assemble a device that could control the process of water heating. A picture of the whole system at rest is reported in Figure 4.10: the removable strain applicator is inside the tank, where other three elements, which are devoted to the temperature changing process, are found. The first component (denoted with 1 in the figure) is the thermo-

Figure 4.10: Complete setup for both temperature and strain measurements: in the middle there is the strain-specific setup, 1) is the thermocouple, 2) the electrical resistance and 3) the air pump.

couple that is connected to a feedback controller: the thermocouple reports the temperature of the water in the tank and the controller change the values to give to the electrical resistance (number 2 in Figure 4.10) in order to change the temperature. The controller (Figure 4.11, where resistance and thermocouple connections to the tank are visible), based upon how fast the temperature changes in the tank and other features, change its parameters in order to reach the desired temperature. In order to avoid a fast cooling (or heating) of the tank when it works at temperatures away from the one to be found in the laboratory, a polystyrene cover is placed over the tank during the measurements to do not have contact with ambient conditions.
Since the resistance is placed in one point of the tank, it is required to move constantly the water to mix the hotter and the cooler water and have a final homogeneous result. This can be achieved using an air pump (like those for aquariums), which is positioned at the opposite side with respect to the resistance, in order to move first the hotter water (number 3 in Figure 4.10).

Figure 4.11: Image of the temperature feedback controller, built on purpose by the Photonic Engineering Group at University of Cantabria in Santander, Spain.

4.2 Data processing

Once the basics associated with the realization of the experimental tests have been described, post processing methods must be implemented in order to treat the Brillouin gain signal and retrieve those useful informations needed to implement, in turn, artificial neural networks. In the following section the decisions taken over the post processing subject will be reported. Comments on its behavior and results will be done in the next chapter.

4.2.1 ANNs: type and MATLAB® implementation

The chosen computing tool for the post processing is again MATLAB®, thanks to its simplicity and practicality, even if it is also famous for its improvable memory management. It is used both for processing data, to choose useful parameters and see how measurements can be improved, and to implement ANNs. In MATLAB®, ANNs can be simply implemented using the Neural Network Toolbox™, so hereafter only the decisions over the type of

ANN used in this thesis will reported.
Based on what was commented in Chapter 3, for this thesis it was decided to choose the most common ANN, i.e. a feedforward neural network with a supervised backpropagation learning algorithm. As training algorithm, the Levenberg-Marquardt optimization was chosen: it is a fast backpropagation algorithm and usually the standard one when the NNToolbox^{TM} is used. As documentation, "it is highly recommended as a first-choice supervised algorithm, although it does require more memory than other algorithms". Last, the decision on whether the training is finished is performed by a minimum squared error performance function.
Many different ANNs, with various number of neurons, hidden layers and training percentages, have been developed for this thesis, in order to understand which one is the best among them to discriminate between temperature and strain contributions. In order to choose these characteristics, some observations must then be done. Usually, for not so complicated tasks, a single hidden layer can do most of the job: too many hidden layers, in fact, could only slow down the performance without adding so much benefit. Also, if the number neurons is too high, there could be the possibility of overfitting the network, directing it to remember the training examples instead of learning from them, in order to generalize when working with new input sets.
Also, measured data are divided into training, validation and test blocks proportionally, trying with different percentages. It is clear that if more input are used as training, the ANN can learn better with higher probability also to generalize. However, if data are not so good, giving many inputs that refers to the same target but with really different characteristics, it may mislead the ANN training and so its creation.

5

Experimental tests

In this chapter experimental tests, measurements and all that has been done in order to achieve and study how discrimination between temperature and strain can be obtained via BOTDA systems, are reported. Obviously, hundreds of measurements were done to adjust the setup, to set how the fiber should be positioned on the supporting tools, to obtain the best possible Brillouin scattering trace, etc. It is anyway clear that not every result will be here described but only those meaningful, from the preliminary stage tests to the final results, in order to explain the whole process that led to the conclusions of this thesis, exploiting the tools shown in the previous chapter.
As before, measurements could be subdivided in three sections: the first, regarding temperature measurements performed in the climatic chamber; the second about strain tests using the ad-hoc configuration and the third, measuring temperature and strain at the same time employing the feedback controlled tank. However, since the first two measurement groups are basically devoted to the study and analysis of the whole measurement setup, to perform good final tests, they will be here subdivided in preliminary measurements and final measurements.
Since tests were performed with different types of fiber and condition, it is not possible to have a brief summary of the parameters of the measuring devices once for all. On the contrary, a more likely step-by-step explanation will be hereafter considered.

5.1 Preliminary settings and measurements

5.1.1 Phase one: temperature measurements

At the beginning of the work for this thesis it was necessary to understand the fiber and stimulated Brillouin scattering behaviors, thus to comprehend how to eventually change setup parameters, fiber placement and so on in case of an undesired outcome. Changing the temperature of the fiber and watching its effect on the Brillouin gain was then perfect in this first phase: not only Brillouin measurements could be done, seeing also the differences in the BGSs due to various temperatures, but even ANNs could be developed initially just to distinguish between the different values, starting to become familiar with them.

After taking confidence with the instrumentation and its characteristics, the first measurement done was the classic Brillouin gain trace along one of the available fibers. A 20 km SMF was here employed, the oscilloscope sample interval was set to 10 ns, the number of measured points were 50000, the number of averages $N_{AV} = 2048$, the rectangular pulse generator frequency was 2 kHz and its amplitude 1 Vpp. The pulse generated from the SOA had a linewidth of about 10 ns to 13 ns, to be little enough to give high spatial resolution (about 1 m) but to do not enlarge too much the Brillouin signal. Part of the BGS along the FUT is represented in Figure 5.1, where it is visible the attenuation of the gain due to normal attenuation of the silica around 1550 nm. The fiber was at ambient temperature, at around 20 °C, while the EDFA was set to obtain a gain of about 20 dB, in order to have enough power for the pump but not too much to deplete it with the scattering process. In this case, since the oscilloscope sample interval was 10 ns, each point of the acquired trace accounted for 1 m of fiber. After this one, some measurements were performed with the climatic chamber. At first, a 30 m spool was retrieved from the end of the optical fiber and inserted into

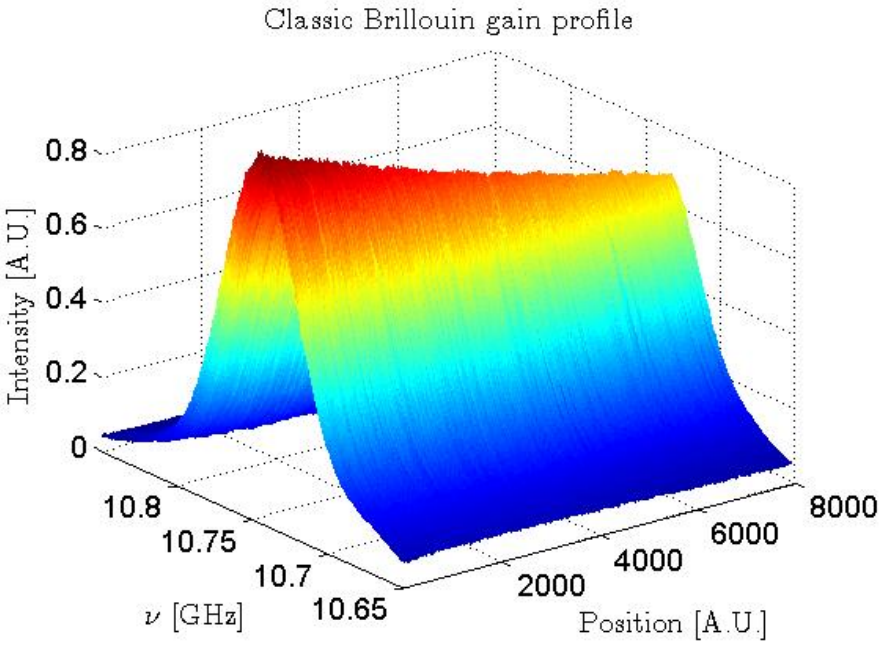

Figure 5.1: Part of the Brillouin gain profile at ambient temperature, for a 20 km G652B/D SMF.

it. It must be said that, if the configuration of Figure 4.1 is considered, the end of the fiber ($z = L$) is where the probe is launched. In that case, since Brillouin gain depends on the pump power, at the end of the fiber the pump has traveled through its entire length and suffered the highest attenuation. For these reasons, having the "hotspot" (i.e. where the fiber temperature or strain is modified) at the end of the fiber is the worst case measurement [2]. For these reasons, once noticed this fact, it was simply necessary to reverse the connections between the fiber and the measurement setup, thus having the hotspot at the beginning of the fiber, where Brillouin gain is at its maximum power.

Measurement range was set in order to reach all the possible frequency shifts: for example, in this case, the oscilloscope central frequency was set to 10.80 GHz with a span of ± 150 MHz, to reach and measure BGSs from

$T = 20$ °C to $T = 90$ °C. In fact, in order to use these measurements as ANNs input, it was necessary to have consistent measurements, with the same frequency range and many other parameters that, if different, could mislead the performance of the ANN.
From these temperature measurements it was possible to retrieve, for example, a representation of different BGSs depending on the temperature of the climatic chamber, similar to the one in Figure 2.3. In Figure 5.2 it is pos-

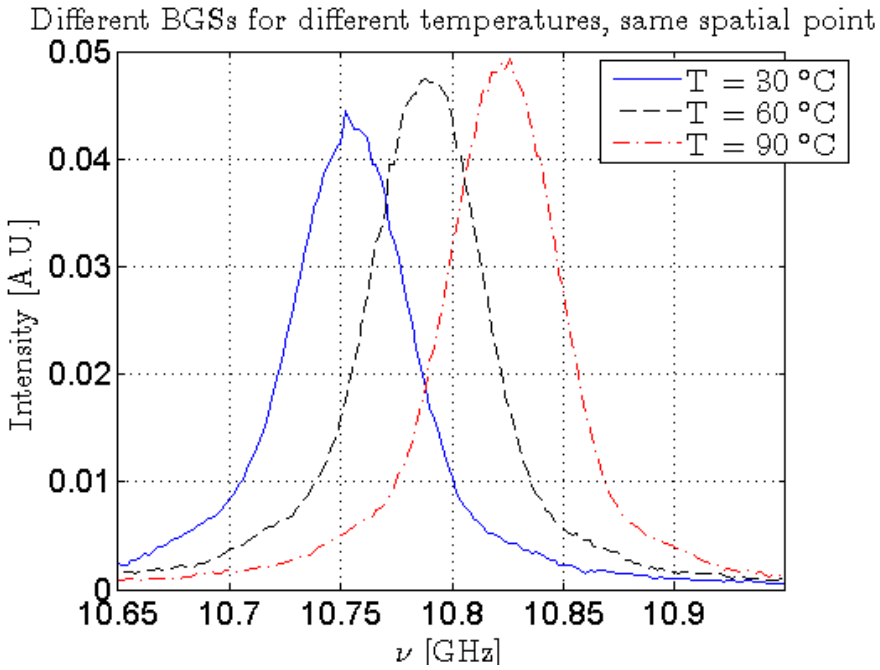

Figure 5.2: Examples of three BGSs, due to three different temperatures.

sible to notice some typical behaviors of the Brillouin gain spectrum when fiber temperature changes, obviously considering the same fiber and same spatial point in order to have coherent data: the central frequency, the so called BFS or ν_B, is shifted to higher values when temperature rises, while also the central peak amplitude changes concordantly with the temperature. A third feature should also be observed: as the peak intensity increases,

since the shared power should be the same, the linewidth of the BGSs should narrow while temperature increases. This is clearly visible in Figure 2.3, however in Figure 5.2 this is nearly observable, where BGSs seem to have same linewidths. There might be different causes for this behavior: this could be due to the specific type of fiber, since each fiber core/cladding materials and doping can give different characteristics to fibers and their behavior. This however is not the only possible reason, therefore some lines will be devoted in the final chapter of this work (Conclusions and future research) in this regard.
Artificial neural networks here were just partially used, specially to understand how they worked and which is the most suitable way to give them inputs. In this phase many tries were done, using some temperatures for the training phase and testing with other measurements at different and intermediate temperatures. In these preliminary features the ANN use will not be explained in detail, it is however worth saying that in this case three or more hidden layers were used, since an higher number of hidden layers always improve the flexibility of the ANN. However, as reported in Chapter 4 and as it will be demonstrated in the following sections, the same performances could be achieved with just one hidden layer, speeding the work.

5.1.2 Phase two: strain measurements

Strain measurements were the second phase of this work: while for temperature measurements there was yet the climatic chamber ready to work, so the measurements were useful to take confidence with the setup, there was not in the laboratory a tool to properly strain the fiber for distributed measurements. Therefore, it was built ad-hoc, as reported in Section 4.1.2.2, and so this phase was more dedicated to understand how to optimally strain the fiber. Also in this case, after some measurements, other tries with ANNs were performed, in order to get closer to the "perfect" type of ANN to be used for the final measurements and goal. As before, most part of the work

with ANNs will be here not reported since it will be all summarized in a succeeding section.

Two SMF G652B/D spools, both of length $L = 2$ km, were fused one with the other, after retrieving 30 m of fiber from one of the spools and rolling it up on the plastic wheels of the strain system. These 30 m were a compromise between having sufficient fiber portion that goes under the strain effect and not having too much fiber to unroll from the coil and roll again onto the new setup, with the risk of breaking it or ruin it and have the necessity of doing the roll up again. In this case, 30 m corresponded to more or less 6/7 rounds back and forth around the system.

Measurements in this case were done with the same BOTDA configuration as before, with exception of the number of averages $N_{AV} = 1024$, reduced in order to speed up the measurement time (from 15 minutes of the previous to about 5) without worsening too much the trace, and the number of acquired samples from the oscilloscope, that was reduced to 10000 since the fiber in this case was shorter. The pulse generator was set to a frequency of 6 kHz and the frequency range at 500 MHz, differently from before, in order to be able to visualize all the frequency shifts due to strain changes. In fact strain was applied by changing the reel in Figure 4.6, starting from 0 turns to reach a higher stress value, for example at 12 turns, where the fiber on the setup was tense like a violin string. One turn of the wheel corresponds to an elongation of 0.5 mm, thus with a simple proportional relation it is possible to see the amount of strain which the fiber undergoes. However, since in this case measurements are performed with span of ± 1 and the values are integers, to use ANNs no transposition is needed and the strain values are just reported as number of turns of the reel.

After the positioning of the fiber on the setup with the metal plates and before the measurements, however, it was needed to do a first ascent/descent cycle applying strain to the fiber, from the lowest to the highest desired value and back, to unstress a bit the fiber from initial constraints and let it adjust on

the wheels. If this action would not be done and measurements started right after positioning the fiber on the wheels, once done the first strain ascent the fiber would surely change its initial stress and thus following measurements, with same amount of turns, would probably give a different scattering behavior and so a different BFS, even with same theoretical amount of strain. In Figure 5.3 a typical Brillouin gain trace is showed, reporting an example

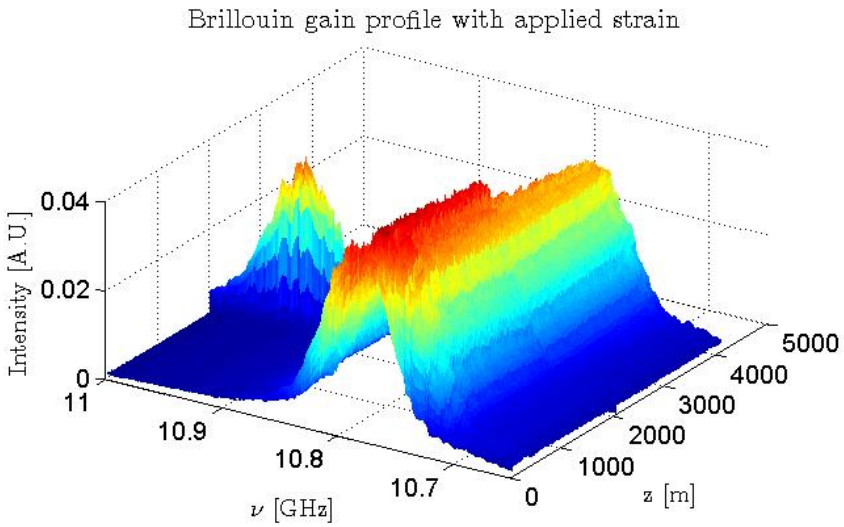

Figure 5.3: Example of a Brillouin gain profile with applied strain on 30 m of fiber.

of an applied strain of 7 reel turns that is visible at the center of the trace were the two fibers are fused together, as some BGSs are shifted in frequency with respect to the ones correspondent to the fiber at rest on the coils. It is also possible to see how the two optical fibers, at their fusion point, have a different intensity (like a step). This could be sign of a loss due to fusion splice or something else, but it was not really relevant after all.
In Figure 5.4 a further detail reporting how much working with this strain setup was sensitive is showed. The choice of retrieving 30 m of fiber to strain was above explained, however it is more immediate to see the difference between a 30 m fiber choice and a shorter one, for example 10 m. It is clearly

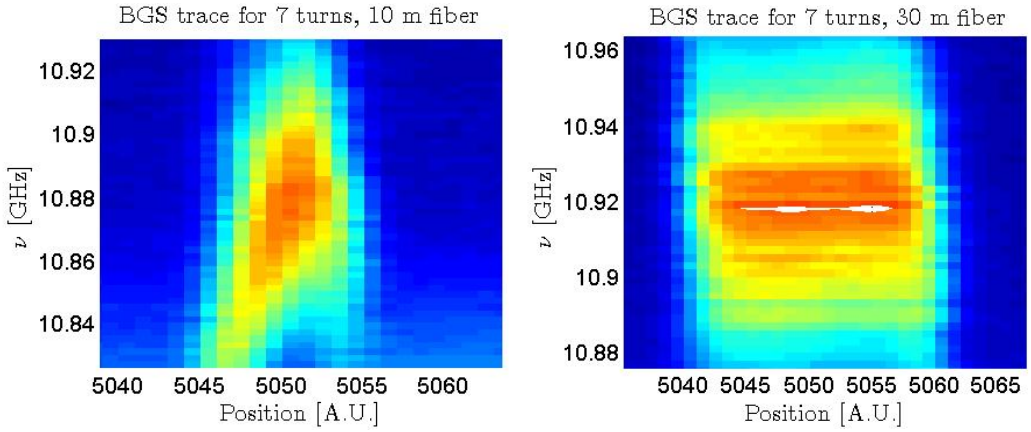

Figure 5.4: Different Brillouin traces for same strain but different amount of fiber.

visible that rolling up to the setup a higher amount of fiber helps the strain being more homogeneous and, also, having more informations for an application to ANNs. Another effect is also noteworthy: the theoretical strain, i.e. the number of reel turns, is equal for both cases (in this case, 7). However, the BFSs of these traces is quite different: one is about at 10.88 GHz while the other at 10.92 GHz, using obviously the same fiber. This is probably due to the different way of rolling up the fiber on the wheels, since doing it manually it was impossible to control how much the fiber was really tensed. A possible solution could have been writing an FBG into the FUT, where it had to be stressed, to sense how much the fiber was manually elongated, however this was too complex to do it rapidly. For these reasons, it was important to try to do the measurements related to a specific set of tests without changing the configuration (thus avoiding breaks, fiber superposition and so on), in order to have the most consistent measurements possible. In this regard, looking at Figure 4.9, it was important to remember to do not let overlap the fiber on itself on the wheels: if it happened, once the fiber was strained, the stress can be felt in different ways in different parts of the fiber, creating a non-regular strain pattern (i.e., more like the 10 m trace than the 30 m one in Figure 5.4).

As for temperature, many strain measurements were done, giving the opportunity to see the dependence of the BGSs with elongation differences. Three

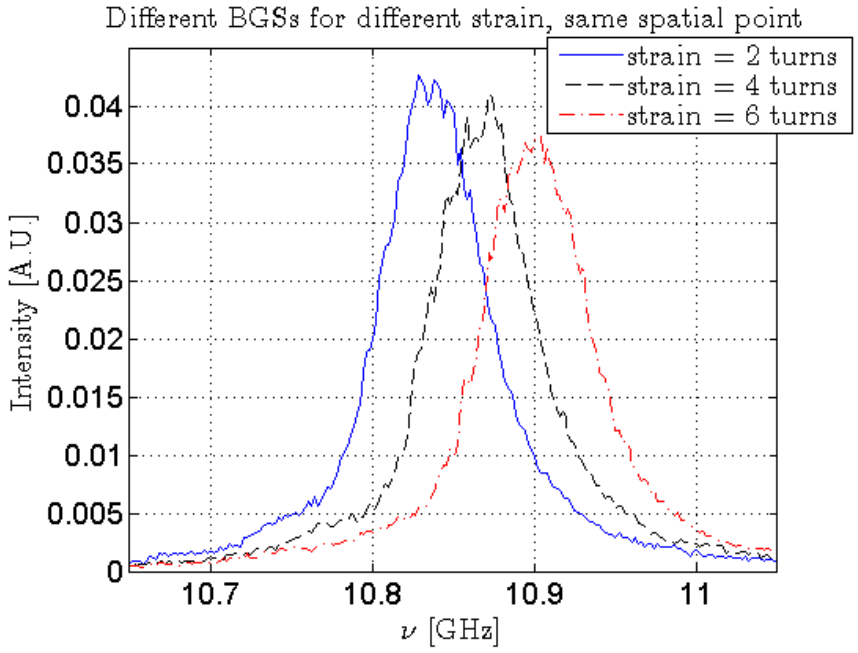

Figure 5.5: Examples of three BGSs, due to three different strain values.

Brillouin gain profiles are represented in Figure 5.5, referring to 2, 4 and 6 reel spins. It represents the same behavior of Figure 2.3: the BFS shifts to higher frequencies with higher strain, the gain amplitude is lowered down and, as for temperature, just very little change in linewidth is visible, probably due to the specific type of fiber or, more likely, to the short pump pulse width selected (as will be explained in the final chapter). It must be said that changes in amplitude and linewidth are really sensitive to little losses or power fluctuations, so it is often difficult to understand if the BGS shape is due to simply Brillouin scattering or something else is occurring.

5.2 Final measurements

Once preliminary measurements were performed and the tank was built, final measurements with the fiber undergoing simultaneous temperature and strain changes were done. This part will be subdivided in three subsections: the first dedicated to physical measurements and their behavior, the second about ANNs and how they were structured in order to perform effect discrimination and the third where results will be reported.

5.2.1 Physical measurements

Final measurements were performed in the tank, illustrated in Section 4.1.2.3, paying attention to roll up the fiber on the wheels in the right way, as commented just before in the previous section. The employed fibers were the same of the strain measurements, retrieving this time ∼20 m to be strained. In this case, referring also to Figure 4.3, the configuration of all the devices was the following : the oscilloscope sample interval is 5 ns, delay time 1 µs, number of samples 10000, full scale 0.5, central frequency 10.8 GHz, range 500 MHz, step 2 MHz, $N_{AV} = 1024$, while the pulse linewidth is ∼12 ns, launched at a frequency of 6 kHz and with an amplitude of 1 Vpp. In this case, since the oscilloscope sample interval was half than previous cases, each trace point was related to 50 cm of fiber. It has to be underlined that, however, this does not give more informations than using a double sample interval, since the pulse linewidth remains the same and so the spatial resolution, but only helps to better visualize the behavior of the Brillouin spectrum.
Measurements were done setting one temperature, since the feedback controlled tank required time to reach the desired temperature and keep it stable, changing then strain from 0 to the highest considered value (like before, a value which gave the fiber a tension like the one of a violin string). After the strain measurements, temperature was set to the following and higher one, until the final considered value. It must be said that the controller was not

so complex and thus worked in a simple way, forcing to set as desired temperature a value a little under the target, since once the electric resistance was heated it was difficult to slow down or invert the process of heating the water, trying then to let reach the target temperature with some kind of residual inertia.
The considered temperature values for ANN training were 20 °C, 29 °C, 38 °C, 46 °C, 54 °C, 62 °C and 70 °C. These values were chosen in order to have almost equally spaced values of about 8 °C, having eventually the possibility to perform other measurements at intermediate temperatures as test data. Strain values were set from 0, where the reel is not turned, up to 10 rounds of the reel that corresponds to an elongation of 5 mm. Each couple of strain/temperature values were measured three times with the BOTDA configuration, in order to have different traces for the same scattering situation.
One of the most problematic issues of this setup was trying to set the desired water temperature. In addition to what has just been commented about the feedback controller, relating to Figure 4.10, an air pump is used in order to mix up the water that was closer to the resistance with the water on the other side that was cooler. Doing some tests, it was noticed that up to 46°C the temperature was quite homogeneous everywhere in the tank also without the support of the air pump. Once the resistance however was quite hot, when the desired temperature was over 50 °C for example, the use of the air pump was almost compulsory, since the difference between ambient temperature and the target one was high. Moreover, the electrical resistance reaches way higher temperatures with respect to the target ones, since it has to heat water rapidly. For these reasons, the air pump was used just from $T = 54$ °C, since it was necessary not only to mix water but also to cool down a bit the resistance, to reach an equilibrium point. Obviously, some tests were done before in order to state that the use (or not) of the air pump was irrelevant on the measurements outcome.

It is important to underline that the temperature was controlled almost every 2-3 minutes by a portable thermocouple, since it was necessary to have a very stable temperature in every point of the tank. Paying the highest attention to this subject, it is however owing to say that the temperature was a little unstable from two points of view: temperature was a bit fluctuating in time, specially for high temperature measurements, of about ± 0.3 °C, while since a wheel was nearer to the electrical resistance than the other, though using the air pump, the water near the resistance was warmer of about 0.5 °C with respect to the further one. In any case, since the frequency shift sensitivity of a standard SMF for temperature is of 1 MHz per degree °C, it is correct to say that these little changes in temperature did not really affect the final results.

5.2.1.1 Analysis of the measured data

Once these training measurements were performed, it was indispensable to analyze them and observe their good and bad characteristics, in order to use them at their best for ANNs implementation. In this regard, since data were the outcome of a 4 km fiber at rest and only 20 m inside the tank were being heated and stressed, it was quite useless to scan the whole fiber length searching for infos. Since the goal is to discriminate between strain and temperature effects, the idea was that giving as input to the ANN both types of fiber trace (outside and inside the tank), it would be able to sense where something was happening and where it was not. However it was quite useless and counterproductive, specially with an eye on ANNs, to give the whole fiber trace as input (having 40 useful point and almost 8000 that were almost equal to themselves), since in this way there was a very little percentage of really useful data. For these reasons, only few points of the fiber at rest were chosen to be reported within the trace used for analysis and ANNs. Only 30 points of the original trace, the ones near to the hotspot, are considered, both before and after the useful and stressed fiber part.

Also, since fiber was manually posed on the configuration, there was a tran-

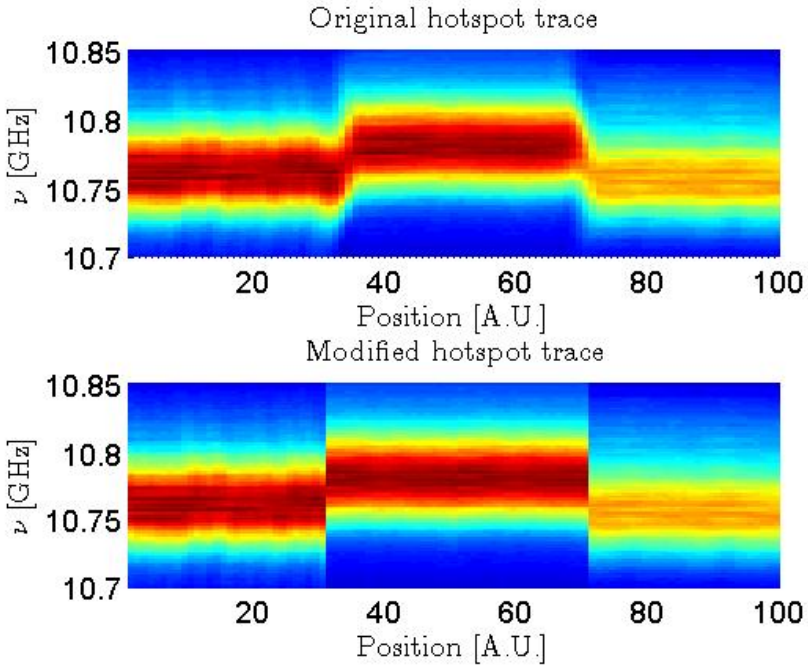

Figure 5.6: Example of the original trace obtained by measurements (on the top) and the modified one (100 points trace) to be treated and be given as input to ANNs (at the bottom). In this case this is referring to the measurement at $T =$ 38°C, with 0 rounds of the reel, so 0 strain.

sition part of the fiber that was between the reeled one around the spool and the one homogeneously rolled up around the wheels. This transition part had also no meaning and did not give any useful information, so it was simply discarded, leaving as trace only the one part which seemed to have a regular outline. In Figure 5.6 the first image is referred to the original trace, zoomed to see the hotspot. The second represents the modified one: it is composed, at the beginning and at the end, only by 30 points of the fiber outside the tank, retrieved from data before and after the hotspot. The transition parts were eliminated and only the very central part of the hotspot

was maintained, constituting 20 hotspot points. These were then repeated twice, in order to increase simply their number. At the end, a 100 points trace was obtained in this case.
As reported many times in this thesis, one of the fundamental characteristics of Brillouin scattering is the shift in frequency of the BFS when the fiber state is altered. Therefore, the first observed features were the BFSs of each point of the fiber, for each strain/temperature value. To perform this, a simple Lorentzian fit was done, in order to obtain the central frequency of each BGS. Referring to the 100 point traces, the map of all BFSs of the measurements, for a fixed temperature and variable strain, is reported in Figures 5.7 and 5.8.
Many comments, specially about the setup and the measurement procedure, can be done just by looking at these images, firstly in a general view: paying attention to a single temperature, grows in strain increase the resulting BFSs, as expected. In the same way, looking at BFS values correspondent to same strain, it is visible that they increase as the temperature grows, as discussed some sections before: if strain or temperatures grows, BFSs grow accordingly. Continuing on this general overview of Figure 5.7 and 5.8, there is also another particular behavior that was however not enlightened until now by the theory: it is possible to notice how for higher strains there is a consequent wavier behavior of the BFS trace. This can be also seen in Figure 5.9, where Brillouin trace of a measurement for $T = 38$ °C and 5 turns of the reel is represented. Here, a clear wavy behavior is visible. This is probably due to a not so perfectly homogeneous strain between the fiber that was left free in the water and the one that was forced onto the wheels. In fact, a similar Brillouin trace is retrieved in [26], where it was generated on purpose by connecting some audio speakers to the fiber, to induce fast strain variations. In this thesis case, this was probably caused by a higher

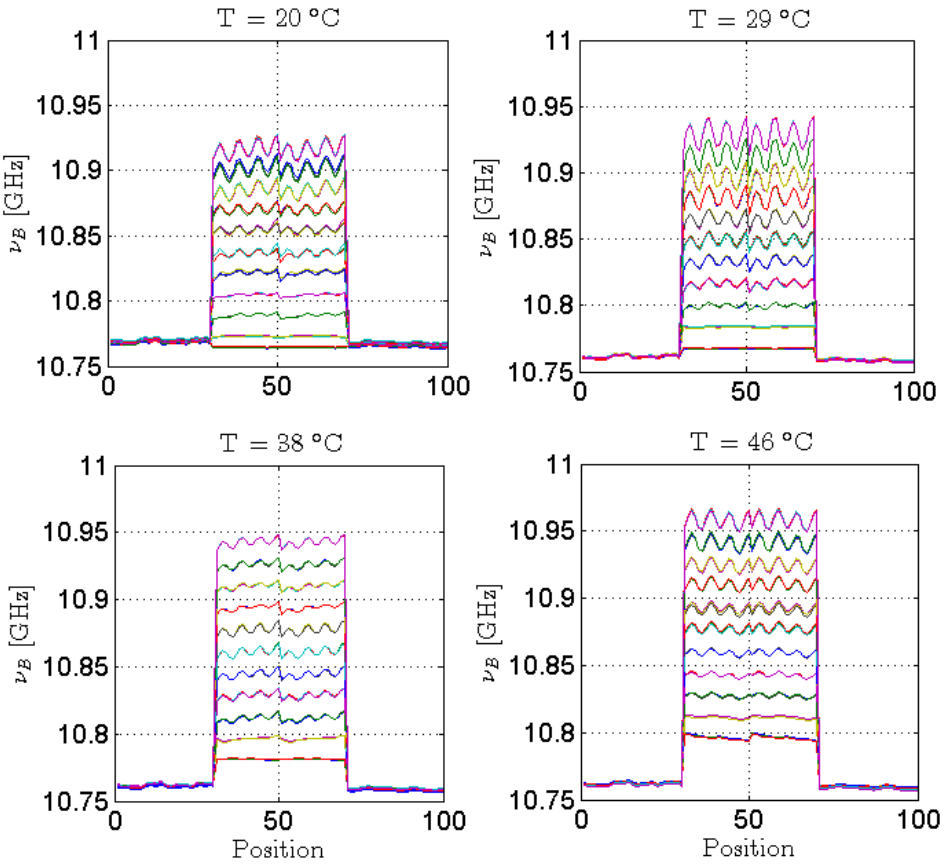

Figure 5.7: Map of the BFSs for $T = 20$ °C, $T = 29$ °C, $T = 38$ °C and $T = 46$ °C. For each temperature, strain from 0 to 10 rounds is represented, where the lowest line is 0 strain and the highest is 10.

fastening of the fiber on the wheels, while in the water it was free to float, specially with low strain. When the strain was higher, the fiber that was free in the water was pulled in a greater way by the wheels, becoming more like many violin strings fixed at the two ends than a long fiber that must be stressed gently all along its length, no matter if it is around the wheels or not. Also, water presence helped moving the fiber, even if the air pump was not functioning. After this explanation, it should be also clearer why, if strain grows, the wavy behavior also increases for the same temperature value.

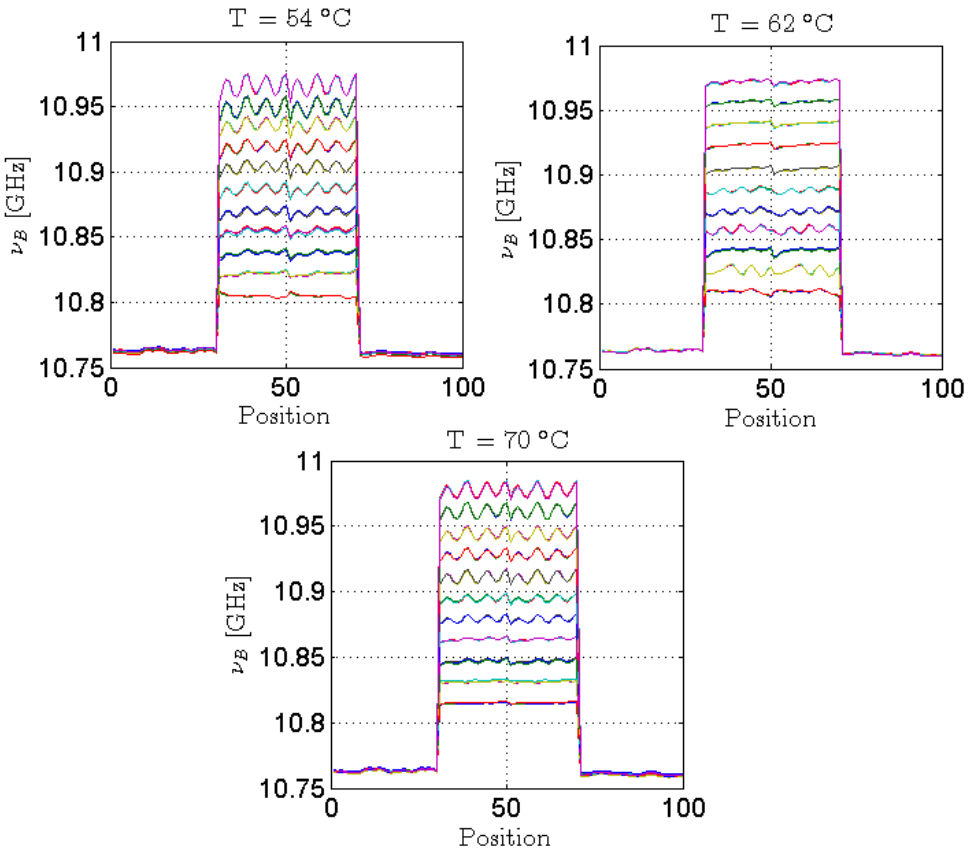

Figure 5.8: Map of the BFSs for $T = 54$ °C, $T = 62$ °C and $T = 70$ °C. For each temperature, strain from 0 to 10 rounds is represented, where the lowest line is 0 strain and the highest is 10.

5.2.1.2 Measurement outcomes issues

After looking at the general behavior, it was then needed to look more into the details of each measurement. It was indeed required to have consistent measurements to have a well trained ANN, so it was also useful to analyze the single measurement and see if its behavior agrees with the others.
One of the first "strange" behaviors concerns the measurements at $T = 20$ °C, reported in Figure 5.7. This was the only test performed without turning on the feedback controller and the electrical resistance, since it was water at

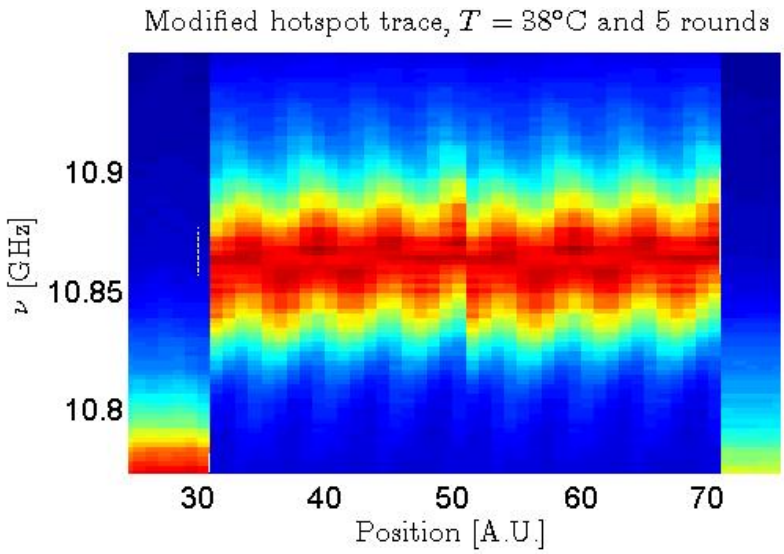

Figure 5.9: Detail of the wavy behavior of a Brillouin trace, example for $T = 38$ °C and 5 spins of the reel.

ambient temperature. For this reason, the temperature was yet more stable, but in one sense also unstable since ambient could vary without control. It can be noticed in Figure 5.7 how the BFSs of the fiber outside the tank is different from the ones associated with other temperature measurements. This can be explained because this measurement was done one week before the others, so the ambient temperature could have been different. In this case, temperature outside the tank was something like $T = 24$ °C, while for the others temperature was $T = 20$ °C.

Starting again by looking at $T = 20$ °C in Figure 5.7, it is possible to see how the 0 strain curve, correspondent to the lowest line in the figure, is not well separated from the other strain lines, as happens for other temperatures. It is also worth mentioning that the fiber coiled on both spools, as well as the one rolled up on the strain system at 0 reel turns, exhibit some strain. In fact, the fibers were mechanically rolled up on bobbins and with a certain precision and velocity in order to do not stress the fiber, while the 20 m fiber was rolled up manually on the system, surely giving the fiber an unwanted

little elongation or stress. In order to have a better strain reference, at first a FBG was rolled up on the system, in order to have a calibrated reference. A detail can be seen in Figure 4.8. However, it broke during the measurements and, as said many times, a try on posing a new one would modify the system configuration, forcing to do again all measurements, also those already performed, so the new ones would not be consistent with the old. For this reason, the measurements continued without the support of the FBG.
Few lines above it was reported how with same strain and higher temperature the BFS increases and that with higher strain the wavy appearance grows. If however the look goes now at Figure 5.8, it is quite immediate to see how the behavior of measurements at $T = 62$ °C is different. In that case two things must be underlined: lines with same strain value, for $T = 54$ °C and $T = 62$ °C are practically overlapped, as if the temperature was not so different during these measurements. Moreover, the waves decrease for higher strains, thus it has an inverse behavior with respect to the previous experiments. The measurement at $T = 70$ °C has a correct wavier trend, however if a linear dependence is supposed to be between temperature and frequency shift, it appears to be more a strain map for $T = 62$ °C and not $T = 70$ °C. A possible explanation of this strange event could be the following: in Figure 5.10, it is possible to see that the inside of the tank, near the electrical resistance, was becoming pink, instead of exhibiting the typical appearance of a metallic surface.
The fiber acrylic coating was also pink, thus letting think that the resistance applied a high temperature on the closest section of the fiber, melting part of its coating that released its color onto the inside surface of the tank. Even though silica optical fiber can stand temperature of a few hundred of degree Celsius, it is possible to say that, starting from $T = 62$ °C (or even before), the heat of the resistance had changed some fiber characteristics and also probably its adhesion to the configuration, altering its original state and behavior. Also, it is necessary to analyze if the water and so humidity had an

Figure 5.10: Inside of the tank on function and detail of its color. The pink is a bit enhanced to let it see in a better way.

impact on these modifications. In [27] application of humidity on Brillouin fiber sensors was studied, obtaining a displacement on Brillouin frequency from 0.4 up to 2.8 MHz, depending of the type of fiber used for measurements. Supported by this argumentation, since from a certain resistance temperature (that is often higher than the target one) water starts to evaporate, it is possible that these particular traces could be due to vapor inside the tank, that during measurements had always on its top a polystyrene cover.

5.2.1.3 Test measurements

As commented at the beginning of this chapter, the initial idea was to give these commented measurements to the designed ANNs as training data, then perform other measurements with intermediate temperature/strain values, within the considered range, to test the resulting ANN. As said, measurements were done by increasing the temperature, from $T = 20$ °C (ambient temperature) up to $T = 70$ °C, observing at high temperatures a little melt of the fiber acrylic coating and subsequent variations in the fiber with respect

to its original state. Temperatures and strain values for test measurements were the following: first, $T = 49$ °C was considered, changing strain as usual. Then, measurements at standard temperatures (from $T = 20$ °C to $T = 70$ °C) were performed, setting the reel to 5.5 spins, that is 2.75 mm of elongation. Once test measurements were done, they were compared with training data. The outcome was clear: comparing for example the same temperature measurements with similar strains (5.5 with 5 and 6, for examples), it was immediate to say that test measurements were not consistent with training ones, having a BFS totally outside the theoretical range. So, the two measurement groups could not be used for the same ANN and so only the first group was used both for training and test (and validation, of course).

5.2.2 ANNs development

Once data were obtained, it was possible to seriously start working with ANNs to achieve the desired temperature and strain discrimination. The general ANN type used for this thesis is reported in Section 4.2.1: a feed-forward ANN with a supervised backpropagation Levenberg-Marquardt algorithm, with a minimum squared error performance function.
In order to get the best possible outcome from the neural network, it is required first to manipulate in a proper manner the Brillouin traces to extrapolate the most important features, then to give those as input to the ANN, to be developed in the best possible way. These two phases will be therefore explained, reporting the chosen process. It has to be said that the training phase of an ANN requires a lot of time, that is higher if the amount of data is bigger, complicating furthermore the analysis of the measurements.

5.2.2.1 Data extrapolation and manipulation

The first move in order to extrapolate useful data from Brillouin traces was already done and reported in section 5.2.1.1: traces were reduced from 8000

to 100 (or less) points, in order to consider only really worthwhile features. In Figure 5.6 at the bottom, the 100 points trace is represented, constituted of 30 points of the part of the fiber just before the hotspot, 40 points made of 20 central points of the hotspot, where strain is more homogeneous (repeated twice) and other 30 points of the fiber just outside the hotspot, always not considering the transition part. Other combinations were studied for ANN applications: for example, to eliminate the FUT that was outside the tank and/or using more data from the central part, for example three or four times instead of two. These different configurations were used based on the amount and type of data that were given as input, as will be next explained. However, the first important things are the removal of the transition part and the little amount of considered BGSs.

Interpolation and normalization

The second thing to do was to interpolate in frequency the traces, in order to have a higher precision when frequency based features were searched (for example the BFS as in the previous sections), passing from the 2 MHz to 400 kHz steps.

Since measurements were performed in different days and probably with slightly different conditions of the devices, it was necessary to transform the traces into the most consistent data possible. So, knowing that a feature that could help discriminate between strain and temperature effects is the amplitude of the Brillouin gain, it was practically compulsory to normalize the traces with the FUT outside the tank, whose scattering power should be the same for each measurement. Normalization was therefore done taking the first 30 points of this new trace, taking the average BGS and dividing the whole trace by the maximum of this single BGS. In this way changes in power due to changes in the setup (input power, EDFA amplification, etc.) should not be a problem.

Input selection: Strips or Lorentzian methods

After these processing, it was necessary to properly select input data for

the ANN, because giving all the BGS curve (of 1251 frequency points after interpolation) would be too much for training. Since the goal is to discriminate between temperature and strain effects and a different dependence of the BGS from them was underlined, proper informations to help the ANN distinguish between the two are surely the BFS, its peak amplitude and its linewidth. Also, ANNs work better with not so many inputs, having then the necessity to reduce to 20/30 points the input data. To do so, two approaches were then considered: the first was to cut into "strips" the curve (called *strips method*), obtaining x-y couple pairs (x = frequency, y = amplitude) of the BGS. These strips were done cutting the shape at preselected percentages of the peak intensity, using for example 0.25, 0.4, 0.5, 0.7, 0.85 and 0.95, obtaining in this way 24 values (two per cut since BGS is a quasi symmetrical curve, in x and y). Since the trace however was not straight but with higher strain it tended to be wavy (Figure 5.9, for example), a simple value to mark the position of each point was made to try to help the ANN to recognize some kind of pattern (marking with a 0 points outside the hotspot and from 0 to 1, with step of 1/20, those 20 points of the hotspot, repeating it if necessary), obtaining a final input vector of 25 points. In this way, indirect informations on the central frequency position/amplitude and the width of the BGS were given to the ANN. The second method is related to the *Lorentzian fitting* of the BGS. After normalization and interpolation, the shape was fitted to a Lorentzian distribution (as to retrieve the BFS in Section 5.2.1.1). Once the fitting shape was obtained, it was possible to recover some useful informations for the training: central peak frequency (the supposed BFS), central peak intensity, width of the shape at 0.2, 0.3, 0.4, 0.5, 0.6 peak intensity percentages, assuming that the difference between the width of the curves with different strain/temperature is more detectable at the base of the Lorentzian curve. With the position info, as before, the input vector in this case was of 8 points.

5.2.2.2 ANN application

Once data for the ANNs are created, it was necessary to build the best ANN possible to reach the goal. To this purpose, different things were to be chosen: the topology of the ANN, i.e. the number of layers/neurons in each layer, how training, validation and test data were selected, how to construct the output vector in order to classify the single inputs and how to treat the ANNs outcome in order to say if it was correct or not.

Hidden layers and number of neurons selection

Based on data and their dimension (depending on how data was taken and given to the ANN, as explained in the previous section), three different type of layers/neurons combinations were done, for each type of data selection (strips or Lorentzian fit), if not stated differently: one hidden layer with same number of neurons as the input layer, thus as input data; one hidden layer with 3 more neurons with respect to input data or two hidden layers with almost equal number of neurons (if data are 25, there will be two hidden layers of 13 and 12 neurons respectively). These values of neurons/hidden layers were chosen for these reasons: usually, for not so complicated tasks, only a hidden layer is necessary. Also, if the neurons are too much, there could be the possibility of overfitting the network, so letting it remember the training examples and not learning from them in order to generalize.

Training/validation/test percentages choice

At this point, since measured traces were specified to be used as training, validation and test sets, it was needed to divide the whole set of data in these three subsets. For this thesis, this was done dividing the whole block of data in three blocks, in a proportional way. It is known that more training data help the ANN to generalize better, however different percentages were used to see the difference in the ANNs work. Training set had the most amount of data, from 50% to 70% of the whole; validation set, depending on training set, was about from 30% to 10% of the total; while test set was the remaining part, between the 20% and 10%. Practically, the tried percentages

were [0.5 0.3 0.2], [0.6 0.2 0.2], [0.6 0.3 0.1], [0.7 0.1 0.2], [0.7 0.15 0.15], [0.7 0.2 0.1].

Training target vector creation

Once ANN and input sets were highlighted, it is now required to explain how the target vector was built, in order to clearly expound how an ANN outcome is considered correct or wrong. In general, an ANN works by classification, selecting the right answer for a determined input from a certain number of possible solutions. So, the output vector used for the training, associated with each single BGS given as input, is made of a sequence of 0 and 1. The first part of the vector represents the possible temperature values and they are as many as the considered temperatures. After that, another vector is attached to its bottom that represents the different classes of strain. For each vector representing a single BGS there will be two 1s: one for the temperature and one for the strain. The rest of the vector is 0 for not correspondent temperature and strain values.

Performance check methods: multiplication, single maximum or two maximums; and final value decision

Finally, before talking about the real ANNs tests and results, it is important to report how the "performance check" was done, so how the output of the ANN was evaluated. In fact, at the end of each training, an ANN is built and ready to be tested. Test inputs were given to this ANN, obtaining as outcome an output vector similar to the one created on purpose for the training but with many different values (and not with 0 or 1 as before). The different approaches to consider the outcome vector were the following: 1) *Multiplication method*: take the output vector, multiply it by the temperature and strain values vectors (like doing a weighted sum), obtaining in this way a temperature and a strain value. Once collected values for each measurement, the values of hotspot points were averaged in order to have an unique value representative of the whole measurement and calculate the error; 2) *Single maximum method*: considering only the maximum (one for

the temperature, one for the strain) and consider the correspondent class as the right temperature and strain values. Then, calculate the error as before; 3) *Two maximums method*: considering not only one, but the first and the second maximums for temperature and strain vectors. Once the two are chosen, for example for the temperature, they were normalized in such a way that their sum gave 1, and then the resulting values are multiplied by the correspondent temperatures to give just one value in the end. Then calculate the error as before.
As a possible change, it was also thought not to perform an average between the hotspot final temperature/strain values but to count the times which a value was spotted. The mean temperature/strain was then the temperature/strain values with more occurrences along the hotspot.

5.2.3 Results

Combining informations obtained in Sections 5.2.1 and 5.2.2, ANNs could be finally developed and the associated results studied. In this final section, all the possible combinations of the previously reported features were tried and the same configuration/data pair was also trained twice in order to have two different networks for the same situation. Errors were simply calculated as difference between the supposed outcome value (using the three methods for the performance check) and the real target one. Then, a success percentage were computed, looking for how many outcomes were near to the target value with a certain precision. Here half of the measurement steps were taken as reference, so an outcome was considered correct if the error in temperature was ≤ 4 °C and the strain error ≤ 0.5. It has to be said that, obviously, errors and success percentages were calculated only based on test block measurements.

5.2.3.1 ANNs trained with all performed measurements

A first try using all the performed measurements was done, using a 100 points trace, both strips and Lorentzian input selection approaches[1], trying with the multiplication and the single maximum method for the output vector and the above mentioned training percentages. Also, an average of the BGSs single results was done to retrieve a single general value. Some comments can be immediately done after this first test: i) Lorentzian method gave a higher successful percentage; ii) a higher amount of training data was better with respect to a lower one, as well as for validation (i.e., with same percentage of training data, more validation data were useful for the ANN building); iii) considering the multiplication method for the performance check was better than selecting the single maximum; iv) only one hidden layer gave better results than using two hidden layers; v) almost always, strain classification was more successful than the temperature one. Some of these comments, as iii) and v) are well represented in Figure 5.11, where only the most successful ANN results are showed. This graphic was done considering an average value for each ANN configuration result, since the simulation was performed twice per each network. The other comments will be confirmed also with other tests later on. The highest success percentages were found using the multiplication method, one hidden layer with same neurons as the input one, for [0.6 0.3 0.1] percentages and using one hidden layer with 4 more neurons for [0.7 0.2 0.1], obtaining respectively 73.9% for temperature, 69.6% for strain and 56.5% for temperature, 78.3% for strain. These values are obtained from a single ANN and not averaged values. Apart from these peak results, the remaining configurations did not give as output many outstanding results, often being around or less than 60% of success for strain and even less for temperature.

[1]In this case, that was the very first one, different strips and Lorentzian amplitudes were used. Proportional values for the Lorentzian one were [0.2 0.3 0.4 0.5], while for strips [0.3 0.5 0.7 0.85 0.95], giving 7 input points for the first and 21 for the second method. For this reasons, also the number of neurons of the hidden layer are different than usual.

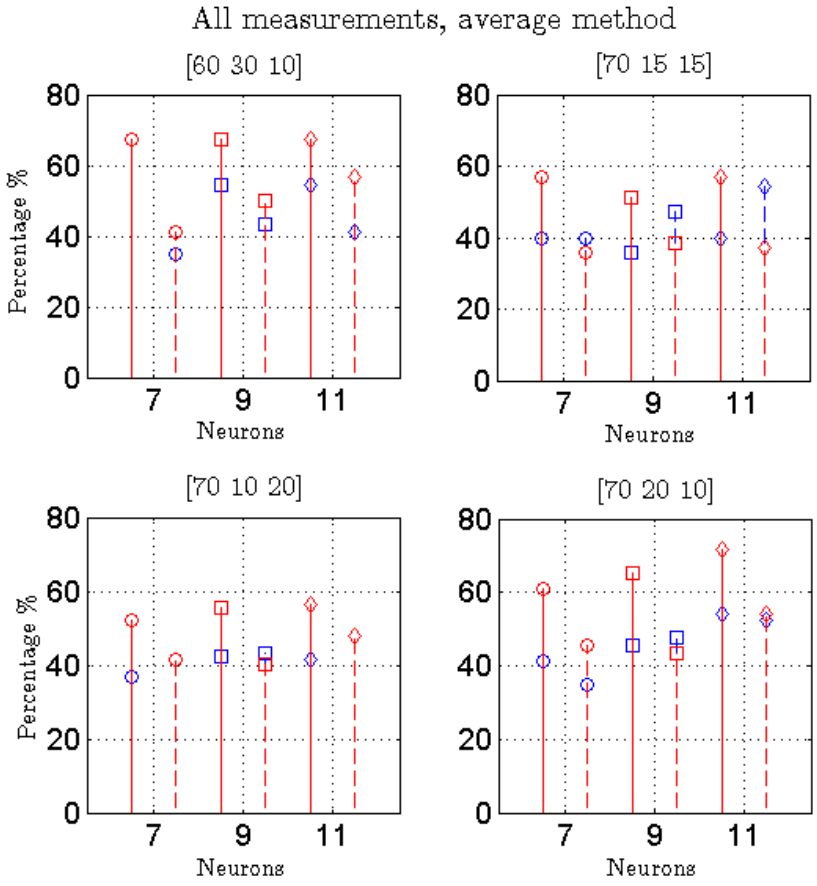

Figure 5.11: Success percentages for some ANN configurations, using all measurements. The legend is the following: blue = temperature values, red = strain; straight line = classic multiplication method, dashed line = single maximum; different marks = number of neurons of hidden layer. Each figure corresponds to a different training/validation/test percentage set, written above.

5.2.3.2 ANNs trained removing erroneous data

It was then necessary to search for other training methods/data to improve these statistics and since it was reported in Section 5.2.1.2 that measurements for 0 strain, 20 °C and 62 °C were a bit strange and not consistent with the others, it was thought to remove them to try to improve classification results.

Removed data: 0 strain and 62 °C measurements

At first, only measurements for 0 strain and 62 °C were discarded and for measurements at 20 °C outside the hotspot was classified as half 20 °C and half 29 °C. In this case, methods/percentages/etc. were like the ones explained in Section 5.2.2 and will remain the same in the following. General results here had a similar trend to the previous case, however looking at single values it was possible to see how in this case they were even worse than the previous ones. This could probably be due to the fact that temperature outside the hotspot for the first set of measurements was unsure, thus saying it was in the middle between 20 °C and 29 °C was probably a mistake. Also, a higher number of data was used in the previous case, helping the ANN to generalize better.

Removed data: 0 strain, 20 °C and 62 °C measurements

For this reason, tests followed up by removing measurements also for 20 °C, introducing then two differences in the ANN configuration with respect to previous examples: the two maximums method was added to the multiplication and single maximum ones, while not only average was performed to decide the general temperature/strain value for a particular trace but also the counting process, as explained at the end of Section 5.2.2.2.

In Figure 5.12 and 5.13 success percentages for the same training/validation/test percentages as before are reported, respectively using Lorentz fitting or strips method to obtain input values. If a classic ANN structure was built, not so many differences could be visible with respect to the previous case, looking at the general behavior. In fact, not a precisely different trend was found, but some success percentages grew, for example temperature ones, while strain ones decreased, for the same training percentages or hidden layers/neurons. This was however the case where higher success percentages were reported: for [0.7 0.1 0.2] training/validation/test percentages, Lorentzian fitted and with one hidden layer of 11 neurons, temperature/strain success

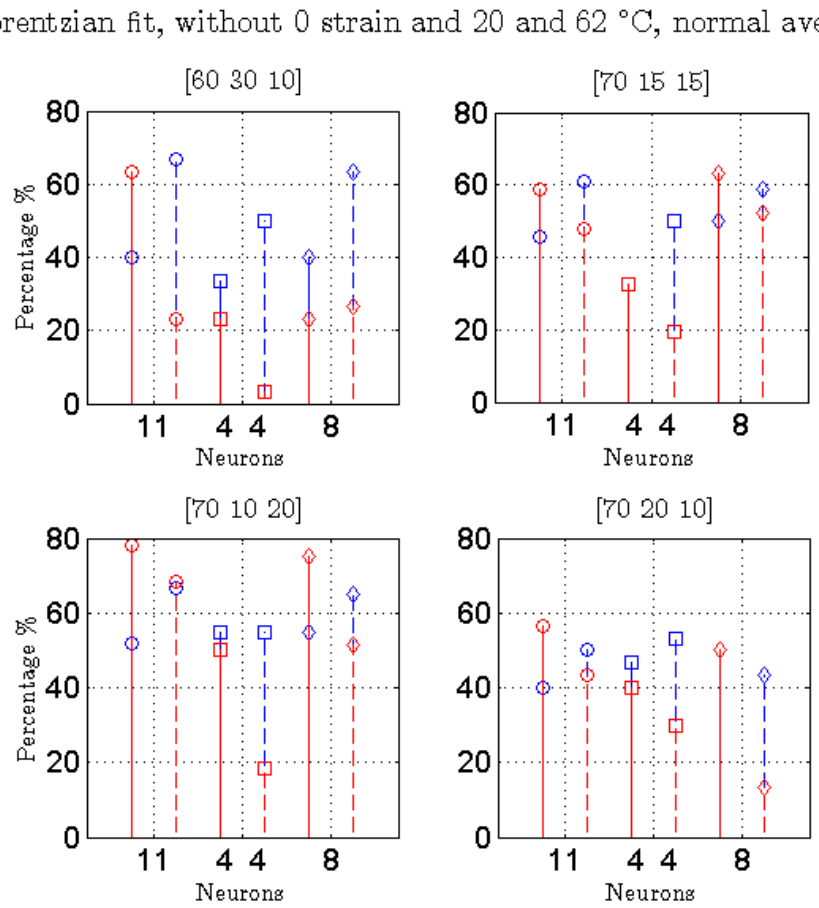

Figure 5.12: Classification ratios for some ANN configurations, not using 0 strain, 20 °C and 62 °C measurements, using Lorentzian fit. The legend is the following: blue = temperature values, red = strain; straight line = classic multiplication method, dashed line = single maximum; different marks = number of neurons of hidden layer. If two numbers are present, it means that there are two hidden layers with respectively those values.

percentages using the multiplication method were 56.7%/86.7% while using the single maximum method were 70%/73.3%. Generally, a higher performance was obtained for [0.7 0.1 0.2] percentages, with respect to previous cases or the same one with different training and validation percentages.

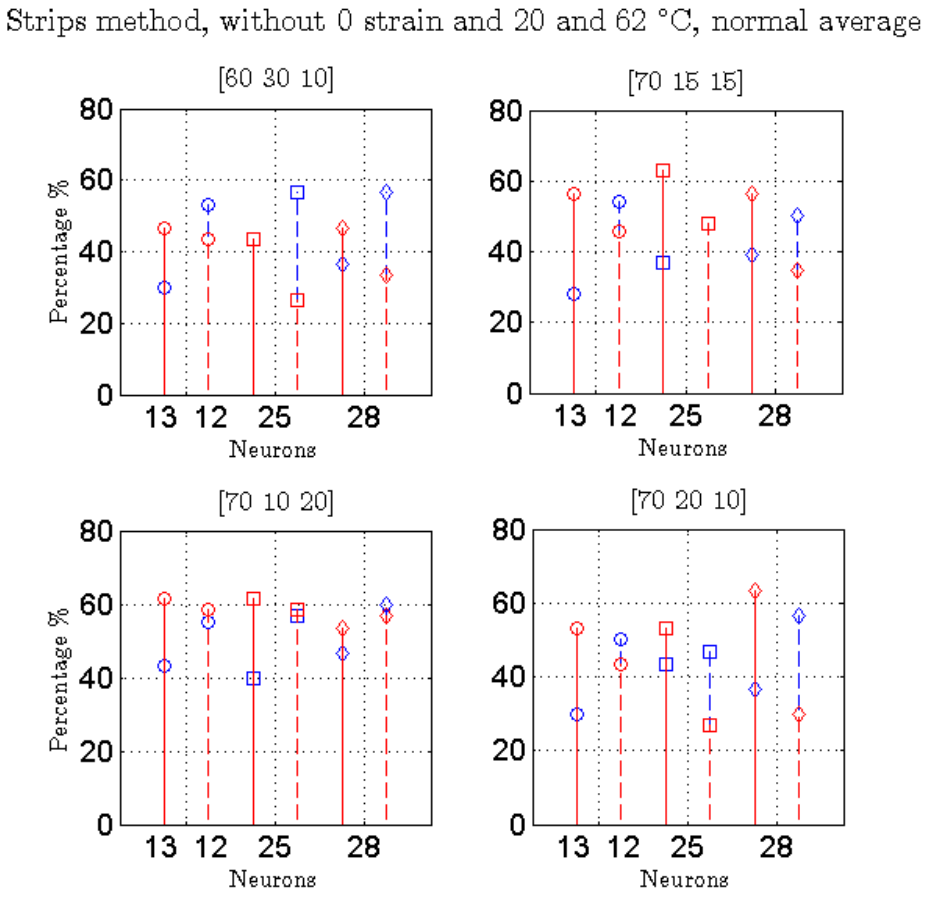

Figure 5.13: Success percentages for some ANN configurations, not using 0 strain, 20 °C and 62 °C measurements, using strips method. The legend is the following: blue = temperature values, red = strain; straight line = classic multiplication method, dashed line = single maximum; different marks = number of neurons of hidden layer. If two numbers are present, it means that there are two hidden layers with respectively those values.

Also, it is possible to see that the general behavior was the same than the one obtained using all measurements: in fact, i) Lorentzian fitting can give a higher success percentage, iv) only one hidden layer gave better results than using two. The other comments can not be done or are just slightly untrue, since using different configurations for the same data can give as out-

put completely different behaviors. Here the average of success, considering only one hidden layer and the highest training percentage, was about 60%, while previously was around 50%.
Using then the two maximums approach to analyze the output vector, not a real difference with respect to the other methods can be appreciated. For some measurements it was better, for some others it was worse, but it did not change dramatically the final results.
If now the counting method is took into consideration, not performing averages of the hotspot values, and coming back to multiplication and single maximum method, the same conclusion as before can be obtained. More precisely, referring to Figure 5.14 where only two percentages of the Lorentzian approach were reported, it can be said that using normal averaging or a counting method to decide which value was the overall one for a single measurement trace (made from more than one BGSs) was not really crucial for achieving the best success percentage. Values are more or less the same, some of them improving and some worsening, however it was not possible to say that one or the other method was better. Probably, the lion's share is done by data selection and not by this process that is only the peak of the iceberg.

Removed data: trace outside the hotspot

Another way to discard the different ambient temperature for 20 °C measurements was to build ANNs using only the hotspot part, constructing a vector of 40 points (twice the 20 points of the hotspot) or 80 points (four times the hotspot). Input data were as always the measurements without the 0 strain and 62 °C case, where some test were done including the 20 °C case and for others it was discarded, since this type of trace was created on purpose in order not to have anymore problems with the 20 °C measurements. In Figure 5.15 comparisons between considering or not 20 °C measurements are reported, were the trace was made of only 40 points and, for example, it was performed the counting process to select the overall final value. In this case

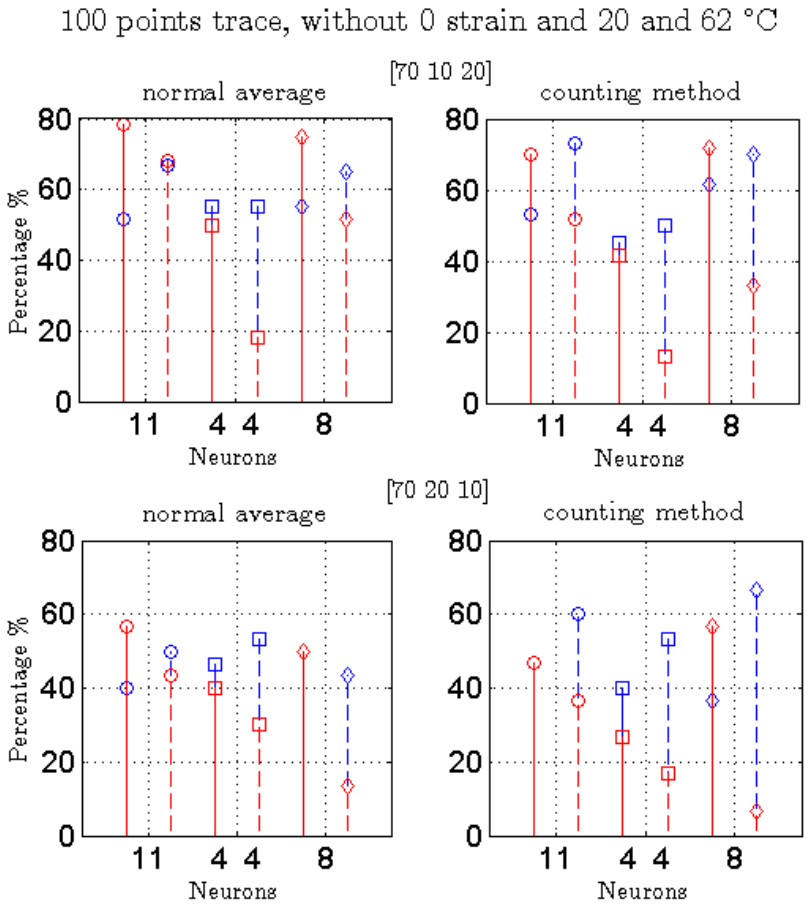

Figure 5.14: Classification ratios for some ANN configurations, not using 0 strain, 20 °C and 62 °C measurements, using both normal average and counting process. The legend is the following: blue = temperature values, red = strain; straight line = classic multiplication method, dashed line = single maximum; different marks = number of neurons of hidden layer. If two numbers are present, it means that there are two hidden layers with respectively those values.

two things are perfectly clear: the first is that not considering 20 °C improves the general success rate, the second is that the maximum approaches, specially the two maximums method, are really bad in some cases, thus letting them be untrustworthy. The test done with 80 points is not even reported,

since its results, also using the 20 °C measurements, were quite disappointing (always going around 30-40% of success at maximum).

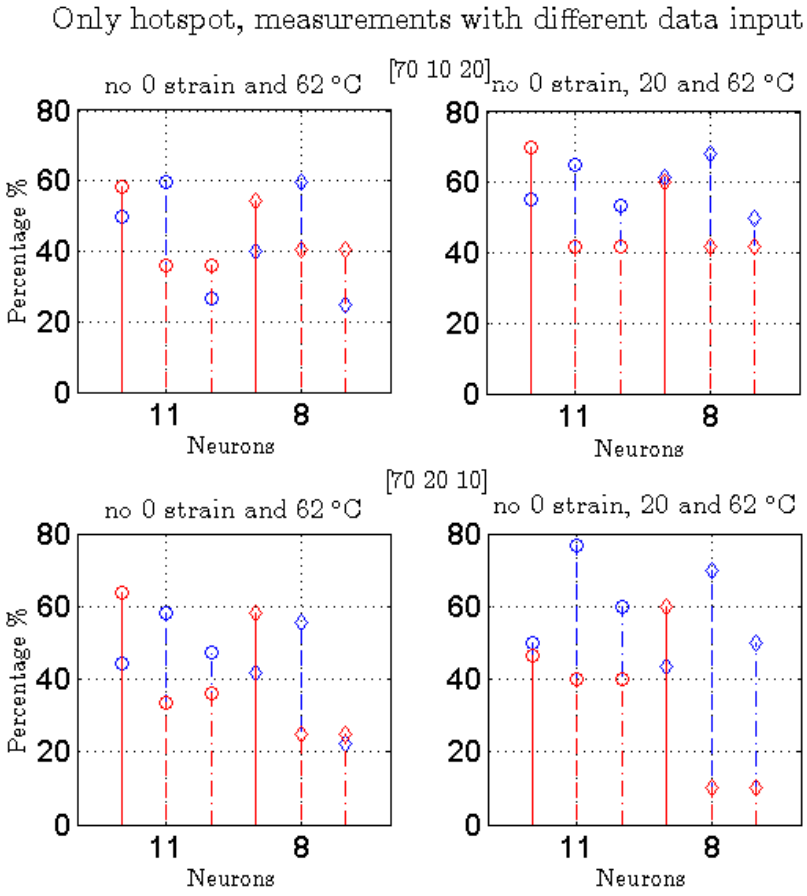

Figure 5.15: Success percentages for some ANN configurations, using only hotspot data, with different input values and counting process. The legend is the following: blue = temperature values, red = strain; straight line = classic multiplication method, dashed line = single maximum, dashed and pointed line = two maximums; different marks = number of neurons of hidden layer.

5.2.3.3 Final comments and summary

In most cases, the configuration which gives the highest classification ratios is the one for training/validation/test percentage of [70 10 20], one hidden layer of 11 neurons, with a performance check done with the multiplication method. The best result is given by removing data for 0 strain, 20 °C and 62 °C for this configuration, regardless if the final value is retrieved doing an average of all values of a single trace or selecting the maximum spotted value within it. Other success percentages are discovered, for example using all measured data, even if it is the case, almost always, for only strain. In general, in fact, strain reaches a higher number of times classification ratios of around or more than 70% (like the outstanding 86.7%) with respect to temperature. In any case, as repeated many times, changing a feature of the ANN (type of input data, hidden layers, training percentages, etc.) does not change temperature or strain success percentages in the same way, not giving a particular tendency. It is finally really important to underline that even if the percentages were not so outstanding (like at 60%), implying that for a lot of traces the error was above half of the measurements step, the ANN was quite often able to follow the measurements. This means that the ANN is in this case able to sense the direction of the difference between the traces (i.e. for example if strain or temperature is increasing between different data), without however being able to perform an accurate quantitative analysis.
Comments, reasons and possible solutions for these observations are reported in the following and last chapter, Conclusions and future research.

6

Conclusions and future research/Conclusioni e sviluppi futuri

English

In previous chapters the developed process in order to achieve the goal of this thesis has been reported and discussed. ANNs have been used to try to perform the desired discrimination between strain and temperature, using informations from the acquired BGSs as input data. Since these were test measurements and not real ones, the true values were known, giving the opportunity to calculate the classification percentages for each case.
Based on the results above reported, some conclusions can be, by now, made: i) Lorentzian fit works better than strips method, even if the second gives more stable solutions as treats a higher amount of data; ii) highest training percentages are the best to achieve good results, even if sometimes also lower ones can give good classification ratios; iii) using only one hidden layer is almost always preferable than using two hidden layers, since results are better or equal and time consumption is less; iv) if some measurements are selected to be removed, it is better to remove all those that are not correct, i.e. it is better to remove also measurements at 20 °C if those for 0 strain and 62 °C are also not considered; v) better results were achieved for training/validation/test percentage of [70 10 20] discarding measurements at 0 strain, 20 °C and 62 °C, obtaining a success percentage of 86.7% for strain using classic multiplication while using the single maximum method a 70%

for temperature; vi) temperature and strain success depends a lot from the performance check method and ANN configuration and often the dependence is not the same, since temperature success could improve changing a parameter while, at the same time, the strain classification could worse; vii) the chosen method to finally retrieve a single value for one measurement trace, between normal averaging or counting process, does not really change the final results, underlying how the most important things are which inputs are given to the ANNs and how the outcomes are managed.

Many reasons can be given to these observations, accompanied with some possible solutions: i) Lorentzian fit gives higher success percentage since it gives a precise notion on where the BFS is, while normally the BGSs are noisy and have not a single highest peak: doing more averages with the oscilloscope could maybe give better BGSs to work with; ii) trivially, giving many training inputs let ANNs learn from more examples, generalizing better everything; iii) this is probably because the task is not so complicated and input values are few; iv) and v), to training properly an ANN it is necessary that all input measurements must be consistent: if all measurements are used, an ANN could be created, even if not perfectly, but it could handle also erroneous data since input data will be a lot. If however erroneous data are planned to be removed, it is important to remove all of them in order to let the ANN learn in the right way. Surely, a higher set of better measurements should have been done here if time was sufficient; vi) temperature and strain success results do not have the same behavior when a feature is changed for the ANN creation and analysis. This could be due to a different dependence from temperature and strain of the fiber and BGS, letting ANNs learn and behave in different ways depending on its characteristics.

Also, since it was used a short pulse of about 12 ns, it could be possible that some useful features (specially variations in the BGS linewidth) were covered and hidden by enlargement of the BGS linewidth due to a wide pulse linewidth (as reported in Section 2.2.2) and not to different environmental

conditions, causing an erroneous outcome of discrimination tests. Using then a 50 ns pulse, for example, it would be possible to have a more classical BGS shape and thus dependence from temperature and strain changes, in order to have the possibility to see clearly a difference in linewidths when the temperature or strain varies.

Apart from these possibilities, some more ways to improve the success percentage to discriminate temperature and strain are hereafter listed and briefly explained. Surely, to do more measurements is the first thing to think about. In the end, the maximum amount of input data given to an ANN was about 23k BGSs, while it is known that ANNs work better using even more examples, in order to learn and generalize in a better way. Also, a thickest set of measurements, performing them with a lower temperature/strain step, would surely help the ANN determine with higher precision the considered temperature/strain value. Different ways to perform these tests would also be: changing the frequency step of the data acquisition, to see if particular differences could be sensed with higher ones, reducing the time consumption; or also try to change the ANN type, as trying to use a feedback one, being helped with its temporal memory characteristics. The mentioned types of input selection were done since some measurements were not consistent with some others: a deeper study on how humidity can affect the measurements and how strain can be performed in a more homogeneous way could be done. Besides this, if the same measurements and configurations would be used, it could be useful to try two things: one is to do an ascent/descent measurement cycle also for temperature, after the strain one. In this way, once reached the highest needed temperature (or more) the fiber acrylic would be yet a bit dissolved and the fiber a little more loose on the strain support, thus once real measurements are performed and temperature is high, it will not critically affect the fiber anymore, resulting in more consistent outcomes also for eventual different test measurements. The second try on this purpose is to perform measurements in an opposite way: in this case, measurements

were performed setting a temperature, changing strain within that value and then change again temperature and so on. In this way, however, highest temperature measurements are performed after many others and the effect on the fiber is seen only after spending some time on them. This approach was used since strain changes were faster than temperature ones, since the water in the tank requires time to be at the desired and also stable temperature. If time however would not have been a problem, measurements performed keeping the strain fixed and changing within that value the temperature, then following changing strain and so on, maybe would have helped to reduce the disequilibrium between low and high temperature measurements, since the fiber would be affected immediately by all range of heat. Obviously, doing everything writing an FBG inside the stressed FUT and looking to its features in order to do consistent measurements would be the best solution. In real life, however, a controlled configuration can not be often obtained, thus forcing future research to study maybe also how fiber react physically to its supports.
These observations are only the main and first ones that came to mind during and at the end of this work. Many others could be made exploring in a deeper way the obtained results. Thanks to these outcomes and associated analysis, it is then possible to assert how this feasibility study on the discrimination of temperature and strain effects on distributed measurements, by means of a BOTDA implementation and a computing tool as ANNs, has been performed with some promising results as no one before did, suggesting that further efforts should be devoted to reach better results.

The results of this work have given rise to the paper "Strain and temperature discrimination in a BOTDA system via Artificial Neural Networks" sent for consideration to OFS25 "25th International Conference on Optical Fiber Sensors", to be held in Korea in April, 2017.

Italiano

Nei capitoli precedenti è stato riportato e discusso il processo sviluppato per raggiungere l'obiettivo di questa tesi. Le reti neurali artificiali sono state usate per provare ad ottenere la voluta discriminazione tra strain e temperatura, sfruttando le informazioni dai BGSs acquisiti e usati come input. Dato che queste erano misure di test e dunque non effettuate sul campo, i valori reali erano noti, dando l'opportunità di calcolare le percentuali di classificiazione per ciascun caso.
In base ai risultati sopra riportati, alcune conclusioni possono essere, per ora, fatte: i) il fit di Lorentz funziona meglio del metodo delle strisce, anche se col secondo si ottengono valori di classificazione più stabili indipendentemente dalla configurazione grazie ad un uso di più dati in input; ii) le percentuali di training più alte sono il meglio per raggiungere buoni risultati, anche se può capitare che anche valori più bassi riescano a portare a risultati soddisfacenti; iii) usare un solo layer nascosto è quasi sempre preferibile rispetto ad usarne due, visto che i risultati sono comparabili o addirittura migliori e il tempo consumato è minore; iv) se si sceglie di rimuovere alcune misure, è meglio rimuovere tutte quele che sembrano non corrette, i.e. è meglio rimuovere anche le misure a 20 °C se quelle a 0 strain e 62 °C sono già rimaste escluse; v) risultati migliori sono stati ottenuti per percentuali di training/-convalida/test del [70 10 20], trascurando le misure per 0 strain, 20 °C e 62 °C, ottenendo una percentuale di successo per lo strain del 86.7% usando una somma pesata mentre un 70% per la temperatura usando il metodo con singolo massimo; vi) il successo nella classificazione di strain e temperatura dipende molto dal metodo con il quale si controlla il vettore in uscita e dalla configurazione della rete e spesso la dipendenza non è la stessa, dato che in alcuni casi il successo in temperatura potrebbe crescere cambiando un parametro mentre, allo stesso tempo, la classificazione dello strain potrebbe peggiorare; vii) il metodo finale per ottenere un singolo valore (di temperatura o strain) che rappresenti una traccia intera, tra una normale media dei

valori ed un conteggio del valore maggiormente presente, non cambia realmente il risultato finale, sottolineando come i fattori più importanti per la riuscita della discriminazione siano la scelta dei dati da conferire alle reti e la gestione del vettore in uscita dalla rete.
Queste osservazioni possono avere molte ragioni, assieme a possibili soluzioni: i) il fit di Lorentz porta ad una più alta percentuale di successo dato che dà una nozione precisa su dove il BFS sia, mentre normalmente i BGSs sono rumorosi e non hanno un singolo picco: facendo più medie con l'oscilloscopio in ricezione si potrebbero ottenere dei migliori spettri di guadagno con cui lavorare; ii) banalmente, se si danno alla rete molti input nella fase di training, questa imparerà da più esempi, aiutandola così a generalizzare meglio; iii) questo è probabilmente perché l'incarico non è così complicato e i valori in input da gestire sono pochi; iv) e v), per allenare in modo appropriato un ANN è necessario che tutte le misure di input siano coerenti: se tutte le misure vengono usate, una rete potrebbe essere creata, anche se non perfettamente, ma potrebbe riuscire a gestire anche dati errati dato che gli input da cui imparare sarebbero molti. Se tuttavia le misure errate sono destinate ad essere tolte, è importante eliminarle tutte in modo da lasciare che la rete si alleni nel miglior modo possibile. Sicuramente, un set migliore (in qualità e quantità) di misure dovrebbe essere stato programmato ed eseguito se il tempo fosse stato sufficiente; vi) i successi in temperatura e strain non hanno lo stesso comportamento quando un elemento della rete, per la creazione o analisi, viene cambiato. Questo potrebbe essere dovuto a una diversa dipendenza da strain e temperatura della fibra e dunque del BGS.
Inoltre, dato che è stato usato un impulso corto, di circa 12 ns, è possibile che alcuni elementi utili (specialmente le variazioni nella larghezza del BGS) siano coperti e nascosti dall'allargamento dello spettro di guadagno di Brillouin, dovuto ad un impulso in ingresso estesosi in frequenza (come riportato nella Sezione 2.2.2) e non a diverse condizioni ambientali, causando un risultato errato di discriminazione. Usando un impulso di 50 ns, per esempio,

sarebbe forse possibile avere spettri di guadagno, e quindi dipendenza da cambi di temperatura e strain, più classici, in modo da avere la possibilità di vedere chiaramente una differenza nella larghezza dello spettro quando la temperatura o lo strain varia.
Oltre a queste possibilità, ulteriori modi per migliorare la percentuale di successo nel discriminare temperatura e strain sono qui di seguito elencati e brevemente spiegati. Sicuramente, effettuare più misure è la prima cosa a cui pensare. Alla fine, la quantità massima di dati che sono stati dati in input alla rete è stata di 23mila spettri di guadagno, mentre è noto che le reti neurali lavorano meglio usando molti più esempi, in modo da imparare e generalizzare in modo migliore. Inoltre, un set di misure più fitto, ottenuto con step di variazione di temperatura/strain più piccolo, aiuterebbe sicuramente la rete a determinare con maggior precisione il valore di temperatura/strain della traccia considerata. Ulteriori modi per effettuare questi test potrebbero essere: cambiare lo step (in frequenza) dell'acquisizione, per vedere se verrebbero rilevate differenze particolari utilizzando step maggiori, velocizzando le misure; oppure provare a cambiare il tipo di rete neurale usato, ad esempio utilizzando una rete in retroazione, potendo sfruttare la sua memoria temporale. Gli input sono stati scelti in una certa maniera perché alcune misure non erano congruenti con altre: uno studio più approfondito su come l'umidità può incidere sulle misure e su come lo strain può essere indotto più omogeneamente potrebbero essere fatti al fine di migliorare i risultati finali. A parte questo, usando le stesse misure e configurazioni, potrebbe essere utile provare due approcci per migliorare il processo: uno è quello di effettuare un ciclo di salita/discesa in temperatura, come già fatto per lo strain, prima delle misure vere e proprie. In questo modo, una volta raggiunta la più alta temperatura desiderata, il rivestimento acrilico della fibra inizierebbe già a dissolversi parzialmente e la fibra risulterebbe un po' più lenta rispetto all'origine, dunque una volta che le misure utili vengono effettuate e la temperatura raggiunge il massimo, questa temperatura non influirà più molto

sulla fibra, potendo ottenere risultati più congruenti anche per eventuali successive misure di test. Il secondo tentativo a questo proposito è quello di effettuare le misure nell'ordine opposto a quello riportato: in questo caso, le misure sono state fatte impostando una temperatura, cambiando lo strain dal suo minimo al suo massimo e successivamente ripetere, cambiando temperatura, fino al raggiungimento del suo valore massimo. In questo modo, tuttavia, la temperatura massima viene raggiunta dopo tutte le altre misure e l'effetto del calore sulla fibra viene rilevato solo dopo un certo numero di esperimenti. Questo approccio è stato usato perché i cambi di strain sono più rapidi di quelli di temperatura, dato che il sistema per scaldare l'acqua necessita di tempo per raggiungere la temperatura desiderata e mantenerla stabile. Se però il tempo non fosse stato un problema, delle misure realizzate tenendo fisso lo strain e cambiando ogni volta temperatura dal minimo al massimo, fino ad arrivare al massimo di strain, avrebbero forse aiutato a ridurre il disequilibrio tra misure a bassa e alta temperatura, dato che la fibra inizierebbe a soffrire immediatamente tutti i valori di temperatura considerati. Ovviamente, in conclusione, compiere tutto scrivendo un FBG all'interno della fibra sotto indagine e fare ad esso riferimento per ottenere misure consistenti sarebbe la soluzione migliore. Nella vita reale, tuttavia, spesso una configurazione controllata non riesce ad essere mantenuta, forzando così le ricerche future a studiare forse anche come la fibra reagisce fisicamente ai supporti su cui è posta.

Queste osservazioni sono solo le principali e prime che sono venute alla mente durante e alla fine di questo lavoro. Molte altre potrebbero essere fatte, esplorando più a fondo i risultati ottenuti. Grazie ad essi e all'analisi svolta, è quindi possibile affermare come questo studio di fattibilità sulla discriminazione degli effetti di temperatura e strain su sensori distibuiti, per mezzo di un'implementazione BOTDA e di uno strumento computazionale come le reti neurali artificiali, è stato portato a termine con alcuni risultati promettenti come nessuno finora ha fatto, suggerendo che ulteriori sforzi dovrebbero

essere fatti per raggiungere risultati migliori.

I risultati di questo lavoro hanno dato luogo al documento "Strain and temperature discrimination in a BOTDA system via Artificial Neural Networks" inviato per considerazione all'OFS25 "25th International Conference on Optical Fiber Sensors", che si terrà in Corea nell'aprile del 2017.

Bibliography

[1] Avi Motil, Arik Bergman, and Moshe Tur. [invited] state of the art of brillouin fiber-optic distributed sensing. *Optics & Laser Technology*, 78, Part A:81 – 103, 2016. The year of light: optical fiber sensors and laser material processing.

[2] Marcelo A. Soto and Luc Thévenaz. Modeling and evaluating the performance of brillouin distributed optical fiber sensors. *Opt. Express*, 21(25):31347–31366, Dec 2013.

[3] T. R. Parker, M. Farhadiroushan, V. A. Handerek, and A. J. Rogers. Temperature and strain dependence of the power level and frequency of spontaneous brillouin scattering in optical fibers. *Opt. Lett.*, 22(11):787–789, Jun 1997.

[4] W. B. Lyons and E. Lewis. Neural networks and pattern recognition techniques applied to optical fibre sensors. *Transactions of the Institute of Measurement and Control*, 22(5):385–404, December 2000.

[5] Kenneth O Hill and Gerald Meltz. Fiber bragg grating technology fundamentals and overview. *Journal of lightwave technology*, 15(8):1263–1276, 1997.

[6] Daniele Inaudi and Branko Glisic. Application of distributed fiber optic sensory for shm. *Proceedings of the ISHMII-2*, 1:163–169, 2005.

[7] John M. Senior and M.Y. Jamro. *Optical Fiber Communications: Principles and Practice*. Prentice Hall Internacional series in optoelectronics. Financial Times/Prentice Hall, 2009.

[8] Xiaoyi Bao and Liang Chen. Recent progress in distributed fiber optic sensors. *Sensors*, 12(7):8601, 2012.

[9] Xin Long Weiwen Zou and Jianping Chen. *Brillouin Scattering in Optical Fibers and Its Application to Distributed Sensors*. InTech, 2015.

[10] K.T.V. Grattan and T. Sun. Fiber optic sensor technology: an overview. *Sensors and Actuators A: Physical*, 82(1):40–61, 2000.

[11] Tony Irujo and Tim West. Coming to grips with loss, fusion splicing guidance for single-mode fibers.

[12] David W. Hahn. Raman scattering theory. *Department of Mechanical and Aerospace Engineering, University of Florida*, 2007.

[13] A. Yeniay, J. M. Delavaux, and J. Toulouse. Spontaneous and stimulated brillouin scattering gain spectra in optical fibers. *Journal of Lightwave Technology*, 20(8):1425–1432, Aug 2002.

[14] M. Nikles, L. Thevenaz, and P. A. Robert. Brillouin gain spectrum characterization in single-mode optical fibers. *Journal of Lightwave Technology*, 15(10):1842–1851, Oct 1997.

[15] Andrey Kobyakov, Michael Sauer, and Dipak Chowdhury. Stimulated brillouin scattering in optical fibers. *Adv. Opt. Photon.*, 2(1):1–59, Mar 2010.

[16] Dieter Garus, Torsten Gogolla, Katerina Krebber, and Frank Schliep. Distributed sensing technique based on brillouin optical-fiber frequency-domain analysis. *Opt. Lett.*, 21(17):1402–1404, Sep 1996.

[17] Kazuo Hotate and Takemi Hasegawa. Measurement of brillouin gain spectrum distribution along an optical fiber using a correlation-based technique – proposal, experiment and simulation, 2000.

[18] K. Y. Song, S. Chin, N. Primerov, and L. Thevenaz. Time-domain distributed fiber sensor with 1 cm spatial resolution based on brillouin

dynamic grating. *Journal of Lightwave Technology*, 28(14):2062–2067, July 2010.

[19] C. C. Chan, W. Jin, A. B. Rad, and M. S. Demokan. Simultaneous measurement of temperature and strain: an artificial neural network approach. *IEEE Photonics Technology Letters*, 10(6):854–856, June 1998.

[20] I.A Basheer and M Hajmeer. Artificial neural networks: fundamentals, computing, design, and application. *Journal of Microbiological Methods*, 43(1):3 – 31, 2000. Neural Computting in Micrbiology.

[21] B. Yegnanarayana. Artificial neural networks for pattern recognition. *Sadhana*, 19(2):189–238, 1994.

[22] A. K. Azad, L. Wang, N. Guo, C. Lu, and H. Y. Tam. Temperature sensing in botda system by using artificial neural network. *Electronics Letters*, 51(20):1578–1580, 2015.

[23] Ireneu Dias, Rui Oliveira, and Orlando Frazão. *Intelligent Optical Sensors Using Artificial Neural Network Approach*, pages 289–294. Springer US, Boston, MA, 2008.

[24] J. Mirapeix, P.B. García-Allende, A. Cobo, O.M. Conde, and J.M. López-Higuera. Real-time arc-welding defect detection and classification with principal component analysis and artificial neural networks. *NDT&E International*, 40(4):315 – 323, 2007.

[25] R. Ruiz-Lombera, J. M. Serrano, and J. M. Lopez-Higuera. Automatic strain detection in a brillouin optical time domain sensor using principal component analysis and artificial neural networks. In *IEEE SENSORS 2014 Proceedings*, pages 1539–1542, Nov 2014.

[26] Yair Peled, Avi Motil, and Moshe Tur. Fast brillouin optical time domain analysis for dynamic sensing. *Opt. Express*, 20(8):8584–8591, Apr 2012.

[27] C. Galindez, F. J. Madruga, and J. M. Lopez-Higuera. Influence of humidity on the measurement of brillouin frequency shift. *IEEE Photonics Technology Letters*, 20(23):1959–1961, Dec 2008.